Magma Evolution of the Sete Cidades Volcano, São Miguel, Azores

CHRISTOPH BEIER[1]*, KARSTEN M. HAASE[2] AND THOR H. HANSTEEN[3]

[1]INSTITUT FÜR GEOWISSENSCHAFTEN, CHRISTIAN-ALBRECHTS-UNIVERSITÄT ZU KIEL, LUDEWIG-MEYN-STRASSE 10, 24118 KIEL

[2]DEPARTMENT OF EARTH SCIENCES, UNIVERSITY OF AARHUS, C. F. MØLLERS ALLÈ 110, DK-8000 AARHUS C

[3]IFM–GEOMAR, LEIBNIZ-INSTITUT FÜR MEERESWISSENSCHAFTEN, WISCHHOFSTRASSE 1–3, 24148 KIEL

The Sete Cidades volcano (São Miguel, Azores) is situated at the eastern end of the ultraslow spreading Terceira rift axis. The volcano comprises several dominantly basaltic pre-caldera eruptions, a trachytic caldera-forming stage and a post-caldera stage consisting of alternating trachytic and basaltic eruptions. The post-caldera flank lavas are more primitive (>5 wt % MgO) than the pre-caldera lavas, implying extended fractional crystallization and longer crustal residence times for the pre-caldera, shield-building lavas. Thermobarometric estimates show that the ascending alkali basaltic magmas stagnated and crystallized at the crust–mantle boundary (∼15 km depth), whereas the more evolved magmas mainly fractionated in the upper crust (∼3 km depth). The caldera-forming eruption was triggered by a basaltic injection into a shallow trachytic magma chamber. Lavas from all stages follow a single, continuous liquid line of descent from alkali basalt to trachyte, although slight differences in incompatible element (e.g. Ba/Nb, La/Nb) and Sr isotope ratios imply some heterogeneity of the mantle source. Major and trace element data suggest similar partial melting processes throughout the evolution of the volcano. Slight geochemical differences between post- and pre-caldera stage lavas from the Sete Cidades volcanic system indicate a variation in the mantle source composition with time. The oxygen fugacity increased from the pre-caldera to the post-caldera stage lavas, probably as a result of the assimilation of crustal rocks; this is supported by the presence of crustal xenoliths in the lavas of the flank vents. The lavas from the Sete Cidades volcano generally have low Sr isotope ratios; however, rocks from one post-caldera vent on the western flank indicate mixing with magmas resembling the lavas from the neighbouring Agua de Pau volcano, having higher Sr isotope ratios. The different magma sources at Sete Cidades and the adjacent Agua de Pau volcano imply that, despite their close proximity, there is only limited interaction between them.

KEY WORDS: crystallization depth; fractionation; stratigraphy; Terceira rift; volcanic stages

INTRODUCTION

Oceanic intraplate volcanoes provide insights into both the composition of the Earth's mantle and processes of magma generation and evolution during magma ascent. Ocean island magmatic systems often develop through several stages of volcanism, in which each stage typically shows a distinct chemical and isotopic composition (Woodhead, 1992). The best studied oceanic volcanoes are those of the Hawaiian islands that have evolved through four stages: (1) pre-shield; (2) shield; (3) post-shield or post-caldera; and (4) post-erosional volcanism (Clague, 1987). Although each stage has distinct geochemical variations (e.g. Chen & Frey, 1983; Abouchami et al., 2000), these different stages are thought to reflect variations in source compositions and melting processes as a result of the movement of the lithosphere across a deep-seated mantle plume (Griffiths & Richards, 1989; Frey & Rhodes, 1993; Frey et al., 1994). The Hawaiian plume is, however, unusually strong, with an estimated plume buoyancy flux of 6·5–8·7 Mg/s, compared with a plume buoyancy flux of 1·2 Mg/s for the Azores (Sleep, 1990). Coupled with a much lower plate

*Corresponding author. E-mail: chb@gpi.uni-kiel.de

velocity for the Azores and other Atlantic island groups such as the Canary Islands and Madeira, melt generation and subsequent evolutionary processes may be distinct from those at Hawaii. The repeated volcanic cycles over periods of millions of years for several Atlantic islands appear to be a direct result of the relatively slow plate movement (e.g. Hoernle & Schmincke, 1993; Geldmacher *et al.*, 2000).

Chemical interaction between ascending magmas and the oceanic lithosphere can occur beneath ocean islands. Geochemical studies have shown that assimilation of old oceanic lithosphere and rocks forming the pedestal of the volcano have important consequences for the interpretation of magma compositions as indicators of the composition of the mantle source (e.g. Thirlwall *et al.*, 1997; Wolff *et al.*, 2000; Hansteen & Troll, 2003). Thus, the ascent of magmas beneath oceanic intraplate volcanoes requires detailed study in order to distinguish primary and contaminated basalts and the different possible magma sources. Although the exceptionally large range of geochemical heterogeneity in the São Miguel lavas has been the subject of several studies (Hawkesworth *et al.*, 1979; Davies *et al.*, 1989; Widom *et al.*, 1997; Haase & Beier, 2003; Widom & Farquhar, 2003), the geochemical evolution of single volcanoes on São Miguel has not yet been investigated.

The primary aim of this work is to describe the temporal magmatic evolution and the compositional variations of the Sete Cidades volcanic system, based on a series of stratigraphically well constrained samples. The Sete Cidades volcanic system has been postulated to represent one end-member of a heterogeneous São Miguel mantle source (Hawkesworth *et al.*, 1979; Widom, 1991; Widom *et al.*, 1997). Our data show a distinct evolution of mafic magmas through the stratigraphy as a result of fractional crystallization processes. We propose a petrogenetic model for the subaerial part of the Sete Cidades volcano (<210 000 years), which emphasizes the importance of both fractional crystallization and mixing processes.

GEOLOGICAL BACKGROUND
Geological setting of São Miguel

The eastern Azores platform is dominated by three major tectonic structures: (1) the East Azores Fracture Zone (EAFZ) in the south; (2) the NW–SE striking Terceira rift axis in the northern part of the platform; and (3) the Mid-Atlantic Ridge (MAR) in the west (Fig. 1). The Terceira rift axis represents the plate boundary between the Eurasian and the African plates (Krause & Watkins, 1970; Luis *et al.*, 1994) and appears to be an ultraslow spreading rift with an extension rate of 2–4 mm/year (Searle, 1980; Luis *et al.*, 1998; Vogt & Jung, 2004). Geochemical studies of volcanic rocks from the islands

and the adjacent MAR suggest the presence of a mantle plume beneath the Azores, which is also influencing the spreading axis (Schilling, 1975a, 1975b; Widom & Shirey, 1996). Seismic tomography data show that there is a negative *P*-wave velocity anomaly beneath the Azores, probably reflecting a mantle plume, which, according to Ritsema & Allen (2003), is restricted to the uppermost 200 km of the mantle, but, according to Montelli *et al.* (2004), extends into the lower mantle.

The island of São Miguel lies at the eastern end of the Azores archipelago (Fig. 1) and consists of four large stratovolcanoes and a region of overlapping volcanic rift zones (Waist Zone) between the volcanoes of Sete Cidades to the west and Agua de Pau to the east (Moore, 1990; Haase & Beier, 2003). São Miguel is situated at the intersection of two regional tectonic lineaments that influence the volcanism on the island. The Sete Cidades volcano at the western end of São Miguel is situated on the Terceira rift axis, whereas the eastern three volcanoes of Agua de Pau, Furnas and Nordeste are aligned along an E–W trend parallel to the EAFZ (Fig. 1). All four volcanoes have been active in the last 100 000 years, although the Nordeste volcano in the far east appears to be extinct and is significantly eroded (Abdel Monem *et al.*, 1975; Feraud *et al.*, 1980; Johnson *et al.*, 1998). Lavas from São Miguel show one of the largest ranges of isotopic compositions known from any oceanic island, with Sr isotope ratios, for example, varying between 0·7033 and 0·7052 (Hawkesworth *et al.*, 1979). The Sete Cidades lavas have distinct compositions compared to rocks from the other three volcanoes, with the lowest Sr and Pb isotope ratios observed on the island (Hawkesworth *et al.*, 1979; Widom *et al.*, 1997). However, these distinctions were based on only three Sete Cidades samples and, thus, do not accurately represent the chemical evolution and compositional span of the volcano.

The stratigraphy of Sete Cidades volcano

Stratigraphic observations of Moore (1990, 1991b) and our own field work (Figs 2 and 3) show that Sete Cidades developed through three major phases of volcanic activity: (1) a dominantly alkali basaltic, pre-caldera, shield-building phase; (2) a trachytic caldera-forming phase; and (3) a mainly trachytic, effusive, post-caldera phase associated with small basaltic flank eruptions (Figs 2 and 3). The pre-caldera stage appears to dominate the volcano evolution, covering a time span from >210 000 years and lasting until the caldera-forming eruptions, which comprise a sequence of explosive eruptions that occurred 36 000, 29 000 and 16 000 years ago (Pacheco *et al.*, 2005). The post-caldera stage thus covers the shortest time-span in the volcano's evolution. Hence, the thicknesses and volumes of the three stages differ accordingly. The thickness of the subaerial pre-caldera stage deposits is estimated from coastal outcrops at Mosteiros and Ponta
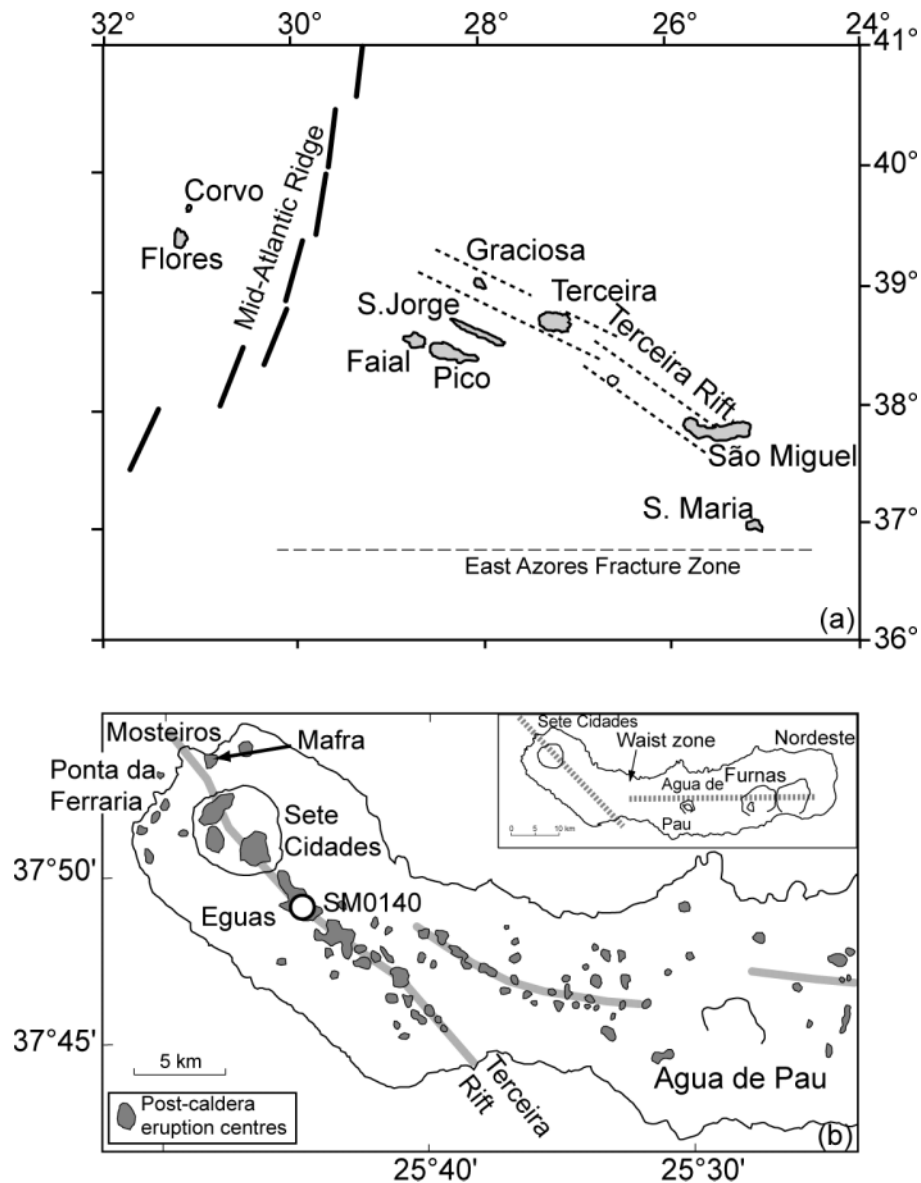
Fig. 1. (a) Map of the Azores archipelago illustrating the Azores islands and associated tectonic features based on Widom and Shirey (1996); (b) map of São Miguel, showing the western end of the island with the volcanic systems of Sete Cidades and Agua de Pau and the post-caldera eruption centres. The sample SM0140 (white circle) was taken from the post-caldera Eguas eruption centre. The inset illustrates São Miguel as a whole and the associated tectonic lineaments (Moore, 1991a). The grey lines indicate the Terceira rift axis and the Agua de Pau scoria cone line.

da Ferraria to be at least 200 m, covering an age range from 74 000 years (oldest unit at Ponta da Ferraria) to 36 000 years (first caldera-related eruption; Fig. 3). However, the maximum thickness of the pre-caldera stage is thought to be significantly larger, because most of the volcano's pre-caldera deposits are either submarine or were covered by younger eruptions. The stratigraphy of Sete Cidades shows several fractionation cycles from basaltic to trachytic compositions over the last 210 000 years (Moore, 1991b) of subaerial activity. For example, the upper stratigraphic section at the sea cliff of Ponta da Ferraria (Fig. 3) shows four changes from basaltic lava flows to trachytic pumice, suggesting that the volcano regularly erupted magmas of different compositions during the pre-caldera stage. The intermediate and evolved magmas erupted from Sete Cidades volcano show ∼11 changes between a basaltic to intermediate and an evolved composition in the last 16 000 years.

The caldera outflow stage comprises a sequence of explosive eruptions producing trachytic airfall deposits and pyroclastic flow deposits that culminated in the caldera collapse. The caldera-outflow deposits have a maximum thickness of 50–60 m at the south-eastern
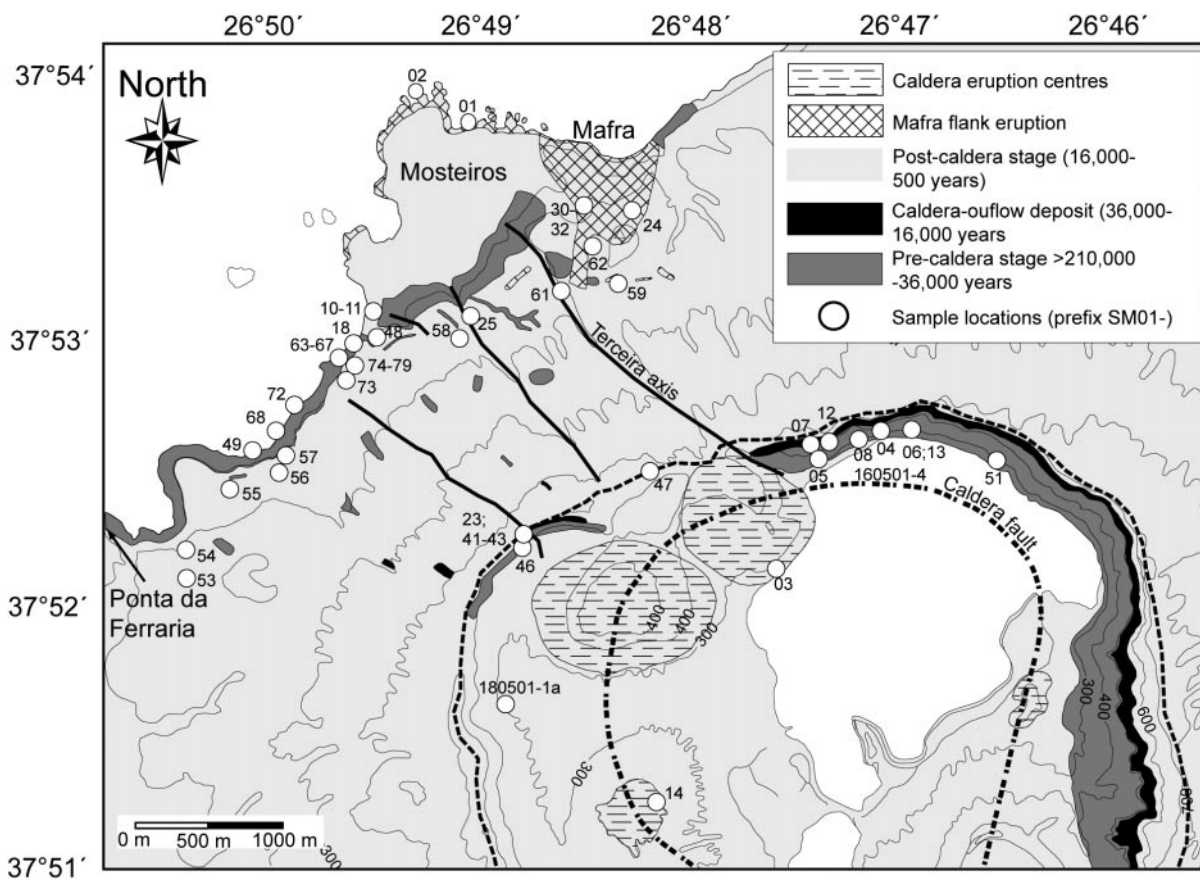
Fig. 2. Simplified geological map of the NW part of the Sete Cidades volcano. The post-caldera stage mainly consists of younger (<16 000 years) pyroclastic deposits covering the pre-caldera lava flows. Sample numbers are related to Table 1, e.g. 10–11 corresponds to SM0110–SM0111. Topographic contours are in 100 m intervals.

caldera rim. The post-caldera ash deposits are generally thicker (up to 40 m) on the south-eastern flank than on the western and north-western flanks (centimetre to metre range), indicating north-westerly winds at the time of eruption (Booth *et al.*, 1978). The trachytic post-caldera stage eruptive units have a variable maximum thickness between 70 and 110 m at the eastern caldera flank and thin out to the metre range in the vicinity of the Mosteiros and Ponta da Ferraria outcrops (Fig. 3). Booth *et al.* (1978) calculated the volume of these explosive eruptions, subdivided into several eruptive events termed Sete A–L, as being up to 3·78 km^3. The explosive post-caldera deposits are intercalated with local basaltic lava flows of variable thicknesses from 2 to 30 m. Although the pre-caldera units are intercalated with thin ash layers of evolved composition, the majority of the pre-caldera stage consists of basaltic and intermediate lavas. In contrast, the post-caldera stage is dominated by larger volumes of evolved pyroclastic deposits and lavas intercalated with smaller basaltic flank eruptions.

The volcano's morphology is influenced by two major tectonic structures: (1) the Terceira rift axis striking through the volcano in a NW–SE direction; and (2) the post-caldera ring fault (Fig. 2). The latter represented a major conduit through which most of the post-caldera trachytes were erupted. On the eastern flank of Sete Cidades, two rows of scoria cones have erupted numerous young lava flows (Fig. 1). The southern row of scoria cones marks a lineament showing a structural connection to the SE-striking Terceira rift axis running through the Sete Cidades volcano (Fig. 1). The Sr isotope compositions of the lavas from these eruption centres indicate that they belong to the Sete Cidades volcanic system (Haase & Beier, 2003). In contrast, the northern row of cones in the Waist Zone strikes more easterly and the lavas have higher $^{87}Sr/^{86}Sr$ suggesting their derivation from the neighbouring Agua de Pau volcano.

SAMPLING STRATEGY AND ANALYTICAL METHODS
Sampling and sample treatment

Selected areas of the Sete Cidades volcano were partly mapped and sampled stratigraphically in May 2001

Fig. 3. Stratigraphy of the Sete Cidades volcano. The localities Ponta da Ferraria and Mosteiros are divided into deposits from the Sete Cidades caldera vent on the left and local flank eruptions on the right. Age constraints are from Moore (1991*a*, 1991*b*) and Moore & Rubin (1991) for the pre-caldera rocks and the flank eruptions, and from Booth *et al.* (1978) for the Sete A–L pyroclastic deposits. The caldera-related deposits were estimated to be 36 000–16 000 years old by Pacheco *et al.* (2005). The vertical axis schematically represents the thickness of each deposit; these vary, especially for the pyroclastic deposits, between individual locations as a result of the influence of the wind during eruption. Sample numbers correspond to the stratigraphic position of the analysed samples.

(Figs 2 and 3). The sampling was carried out based on our stratigraphic investigations and previous studies of the evolution of the subaerial volcanic activity of Sete Cidades (Booth *et al.*, 1978; Moore, 1990; Moore, 1991*b*). Most samples are optically fresh and lack alteration of olivine crystals and vesicle fillings. However, a few samples show signs of a hydrothermal overprint with iddingsitized olivine rims and clay mineral fillings in cracks and vesicles. Glass was present in a few lavas, pyroclastic deposits and scoria samples and, wherever possible, this glass was separated, hand-picked, washed and used for the geochemical analyses. Where glass was not present, fresh cores of whole-rock samples were cut, coarse crushed, washed thoroughly in deionized water, and then fine crushed in an agate ball mill.

Major and trace element analysis

For whole-rocks, 0·6 g of dried powder were mixed with lithium tetraborate and ammonium nitrate, fused to a homogeneous glass bead, and analysed for major element concentrations using a Philips 1400 XRF spectrometer calibrated against international rock standards. Analyses of the samples and international rock standards are presented in Table 1. Precision for most elements was better than 0·8% and accuracy better than 1% of the measured values. The whole-rock FeO^T concentrations used in this work were calculated from the measured Fe_2O_3 contents (Table 1; $FeO^T = Fe_2O_3 \times 0\cdot8998$).

Trace element analyses of whole-rocks and selected glasses were carried out using an Agilent 7500c/s Quadrupole Inductively Coupled Plasma Mass

Table 1: Selected major element, trace element and Nd–Sr isotope data of the Sete Cidades lavas and international rock standards

Sample no.	SM0104	SM0106	SM0116	SM0120	SM0133	SM0134	SM0136	SM0176	SM160501—4	SM0114
Location	NNW-cald. wall	N-cald. wall	Ponta da Ferraria	Ponta da Ferraria	Ponta da Ferraria	Ponta da Ferraria	Ponta da Ferraria	Cliffs in Mosteiros	N-cald. wall	Caldeira seca
Long. (°N)	37·525	37·526	37·516	37·515	37·516	37·516	37·516	37·532	37·528	37·518
Lat. (°W)	25·474	25·468	25·516	25·513	25·516	25·516	25·516	25·493	25·468	25·481
Volcanic stage	pre-caldera stage	pre-caldera stage	pre-caldera stage	pre-caldera stage	pre-caldera stage	pre-caldera stage	pre-caldera stage	pre-caldera stage	pre-caldera stage	post-caldera stage
TAS classification	Basalt	Trachyandesite	Basalt	Trachyandesite	Basalt	Basaltic	Basalt	Basaltic trachyandesite	Basalt	Trachyte
wt %										
SiO_2	46·71	61·23	46·09	58·16	47·09	54·56	46·85	50·08	46·17	63·28
TiO_2	2·98	0·72	3·55	1·27	3·40	1·92	3·17	2·61	3·49	0·49
Al_2O_3	14·05	17·64	14·74	17·99	13·33	17·35	11·89	16·87	14·18	15·56
Fe_2O_3	10·94	3·02	11·81	4·87	11·60	7·33	11·47	9·16	12·01	3·16
MnO	0·18	0·17	0·18	0·17	0·17	0·19	0·17	0·18	0·17	0·24
MgO	7·51	0·48	6·85	1·24	8·60	2·41	10·63	3·75	6·38	0·23
CaO	9·96	1·46	9·92	3·23	11·03	4·86	11·96	7·35	10·76	0·50
Na_2O	2·95	6·85	3·08	5·81	2·83	5·63	2·48	3·73	3·02	7·72
K_2O	1·80	5·17	1·80	4·31	1·58	3·61	1·38	2·65	1·47	5·10
P_2O_5	0·69	0·09	0·59	0·31	0·57	0·62	0·52	0·92	0·52	0·05
LOI	0·51	0·15	0·00	0·47	0·00	0·03	0·11	2·34	0·71	2·30
Total	98·28	96·98	98·61	97·83	100·20	98·51	100·63	99·64	98·88	98·63
(ppm)										
Sc	20·2	1·91	22·4	2·76	28·1	5·63	28·4	9·77	22·2	2·20
V	226	10·4	271	48·0	297	95·0	261	156	299	2·97
Cr	344	1·07	162	2·87	449	1·38	662	12·0	211	1·39
Co	35·8	0·58	40·8	3·43	44·9	8·28	47·4	17·5	41·9	6·06
Ni	117	0·26	57·4	0·72	122	0·39	198	7·27	77·1	0·30
Cu	54·8	1·53	43·8	2·28	67·8	3·42	87·7	10·9	95·3	0·99
Zn	101	92·1	104	97·7	98·7	113	88·4	105	110	154
Mo	2·24	2·06	2·44	3·76	2·02	2·57	1·56	1·55	2·22	11·2
Rb	39·8	133	40·9	102	39·0	86·1	31·6	56·7	20·6	177
Sr	786	313	833	743	715	814	638	893	733	4·14
Y	28·7	39·7	26·3	36·8	28·2	41·8	21·7	33·5	26·6	64·0
Zr	321	808	336	646	305	572	238	414	305	1214

Sample no.	SM0104	SM0106	SM0116	SM0120	SM0133	SM0134	SM0136	SM0176	SM160501–4	SM0114
Location	NNW-cald. wall	N-cald. wall	Ponta da Ferraria	Ponta da Ferraria	Ponta da Ferraria	Ponta da Ferraria	Ponta da Ferraria	Cliffs in Mosteiros	N-cald. wall	Caldeira seca
Long. (°N)	37·525	37·526	37·516	37·515	37·516	37·516	37·516	37·532	37·528	37·518
Lat. (°W)	25·474	25·468	25·516	25·513	25·516	25·516	25·516	25·493	25·468	25·481
Volcanic stage	pre-caldera stage	pre-caldera stage	pre-caldera stage	pre-caldera stage	pre-caldera stage	pre-caldera stage	pre-caldera stage	pre-caldera stage	pre-caldera stage	post-caldera stage
Nb	73·5	166	74·1	148	60·7	130	56·5	98·3	68·1	272
Cs	0·36	0·29	0·29	0·51	0·23	0·62	0·25	0·20	0·28	1·78
Ba	571	1398	502	1301	518	1008	381	752	484	6·84
La	50·5	98·8	48·8	87·6	42·5	81·3	37·0	68·4	45·5	137
Ce	106	190	102	170	88·3	164	78·9	138	91·0	265
Pr	12·9	19·0	12·5	19·3	11·0	19·1	9·74	16·1	11·1	28·6
Nd	51·2	63·4	49·2	69·8	44·1	71·6	39·1	61·2	43·8	95·0
Sm	10·2	10·3	9·65	12·2	8·82	13·4	7·88	11·6	8·74	16·4
Eu	3·04	2·88	2·89	3·60	2·67	3·98	2·36	3·40	2·65	2·47
Gd	8·64	7·92	8·06	9·82	7·54	11·2	6·63	9·56	7·52	13·1
Tb	1·23	1·23	1·13	1·41	1·08	1·62	0·94	1·35	1·08	2·11
Dy	6·44	6·65	5·94	7·66	5·57	8·81	4·83	7·20	5·71	12·2
Ho	1·16	1·26	1·05	1·44	0·98	1·62	0·86	1·29	1·02	2·41
Er	2·91	3·52	2·62	3·83	2·45	4·23	2·10	3·28	2·58	6·73
Tm	0·38	0·51	0·33	0·53	0·31	0·57	0·27	0·43	0·33	0·98
Yb	2·30	3·42	2·07	3·42	1·93	3·54	1·62	2·67	2·03	6·43
Lu	0·32	0·50	0·28	0·50	0·27	0·50	0·23	0·38	0·29	0·93
Hf	7·59	14·4	7·71	13·9	6·33	12·4	6·01	9·03	6·98	26·8
Ta	4·67	8·28	4·72	8·32	3·64	7·62	3·58	5·94	4·23	15·5
Pb	2·46	7·13	2·22	6·61	2·04	4·44	1·64	3·51	2·30	10·6
Th	5·81	15·3	5·33	12·8	4·57	11·0	3·87	8·00	5·80	23·8
U	1·38	3·49	1·53	2·99	1·24	2·84	1·14	2·15	1·63	6·53
$^{87}Sr/^{86}Sr$	0·70353	0·70359	0·70334	0·70365	0·70327	0·70348	0·70340	0·70351	0·70363	0·70418
$^{143}Nd/^{144}Nd$	0·51290	0·51291	0·51292	0·51290	0·51292	0·51290	0·51292	0·51291	0·51291	0·51291

Table 1: continued

Sample no.	SM220501−1	SM0203	SM9704−a	SM9710	513DS−1	515DS−1	SM0101	SM0102	SM0161
Location	N of Ginetes, flank vent	Pico da Pintona	Relva, Waist Zone	Serra Gorda Waist Zone	W-flank subm.	W-flank subm.	Mafra flank vent	Mafra flank vent	Mafra flank vent
Long. (°N)	37·514	37·798	37·750	37·820	37·866	37·865	37·539	37·540	37·534
Lat. (°W)	25·504	25·701	25·710	25·739	25·938	25·998	25·490	25·492	25·485
Volcanic stage	post-caldera stage	post-caldera stage	post-caldera stage	post-caldera stage	post-caldera stage	post-caldera stage	post-caldera stage	post-caldera stage	post-caldera stage
TAS classification	Trachyte	Basalt	Basalt	Basalt	Basalt	Trachyte	Basalt	Basalt	Basalt
wt %									
SiO_2	61·98	46·56	45·71	46·39	46·95	59·29	44·87	45·47	45·36
TiO_2	0·78	2·43	3·44	3·00	2·74	1·28	3·08	2·74	3·59
Al_2O_3	16·88	12·52	12·76	12·64	12·33	18·69	10·96	10·25	13·05
Fe_2O_3	3·42	11·18	12·75	11·91	11·06	5·93	11·96	11·34	12·44
MnO	0·19	0·16	0·17	0·17	0·17	0·19	0·17	0·16	0·18
MgO	0·64	10·42	9·81	10·55	12·13	1·58	12·26	14·09	9·14
CaO	1·16	11·58	11·14	11·27	10·97	3·53	11·62	10·52	10·81
Na_2O	6·94	2·67	2·55	2·45	2·56	5·99	2·11	2·01	2·76
K_2O	5·21	1·15	1·06	1·22	1·38	4·32	1·19	1·40	1·26
P_2O_5	0·15	0·40	0·52	0·48	0·48	0·38	0·52	0·45	0·69
LOI	1·13	0·23	0·00	0·00	0·00	0·00	0·00	0·00	0·00
Total	98·48	99·30	99·91	100·08	100·77	101·18	98·74	98·43	99·28
(ppm)									
Sc	29·8	31·2	19·9	26·1	24·1	3·16	30·9	29·0	24·4
V	22·7	262				40·6	263	229	289
Cr	6·78	788	670	784	996	2·25	654	705	405
Co	7·34	50·3	48·6	41·1	44·6	4·95	55·8	59·7	47·1
Ni	2·47	212	185	289	319	1·75	225	311	139
Cu	2·53	86·2	25·9	99·4	70·5	3·29	83·5	74·9	36·7
Zn	115	89·7	82·6	95·0	90·0	92·1	85·0	84·3	99·0
Mo	6·37	1·71	1·86	1·63	1·90	0·97	1·68	1·84	1·99
Rb	95·0	33·3	22·6	24·3	28·5	1090	27·1	32·3	33·1
Sr	110	527	615	594	622	543	589	534	797
Y	37·1	25·8	23·2	19·1	19·3	33·7	20·4	19·5	25·4
Zr	698	177	207	168	259	607	200	226	248
Nb	168	40·9	45·7	39·7	48·0	130	43·6	44·8	57·4
Cs	0·95	0·40	0·05	0·30	0·32	0·26	0·25	0·28	0·32
Ba	730	411	359	364	404		347	348	494
La	76·4	28·0	30·5	30·5	36·6	89·5	32·5	33·5	40·9
Ce	152	57·8	64·6	64·1	75·5	173	69·3	71·4	86·5
Pr	17·0	7·26	8·04	8·12	9·51	19·4	8·71	8·85	10·8

Sample no.	SM220501−1	SM0203	SM9704−a	SM9710	513DS−1	515DS−1	SM0101	SM0102	SM0161
Location	N of Ginetes, flank vent	Pico da Pintona	Relva, Waist Zone	Serra Gorda Waist Zone	W-flank subm.	W-flank subm.	Mafra flank vent	Mafra flank vent	Mafra flank vent
Long. (°N)	37·514	37·798	37·750	37·820	37·866	37·865	37·539	37·540	37·534
Lat. (°W)	25·504	25·701	25·710	25·739	25·938	25·998	25·490	25·492	25·485
Volcanic stage	post-caldera stage	post-caldera stage	post-caldera stage	post-caldera stage	post-caldera stage	post-caldera stage	post-caldera stage	post-caldera stage	post-caldera stage
Nd	59·9	29·5	33·5	33·4	38·3	68·0	35·5	35·5	44·3
Sm	10·5	6·44	7·13	7·32	7·93	11·8	7·37	7·17	8·97
Eu	2·69	2·04	2·22	2·27	2·43	3·32	2·25	2·13	2·77
Gd	8·41	5·92	6·61	6·36	6·70	9·65	6·40	6·04	7·59
Tb	1·31	0·90	0·92	0·92	0·96	1·44	0·91	0·86	1·07
Dy	7·38	4·92	4·97	5·12	5·16	7·76	4·75	4·51	5·60
Ho	1·41	0·89	0·89	0·94	0·93	1·44	0·84	0·80	1·00
Er	3·85	2·23	2·19	2·30	2·28	3·81	2·09	1·97	2·47
Tm	0·55	0·29	0·28	0·30	0·29	0·54	0·27	0·26	0·31
Yb	3·55	1·84	1·70	1·75	1·76	3·49	1·62	1·57	1·90
Lu	0·50	0·26	0·24	0·24	0·24	0·50	0·21	0·22	0·26
Hf	14·5	4·37	5·36	5·33	5·98	15·1	5·43	5·95	5·94
Ta	9·08	2·47	3·04	2·89	3·34	8·73	2·86	2·94	3·65
Pb	6·26	1·85	1·93	1·86	2·05	6·13	1·59	1·84	1·80
Th	11·9	3·33	3·67	3·42	3·82	13·5	3·33	3·73	4·06
U	3·19	0·89	1·08	1·04	1·14	1·76	0·89	1·00	1·06
$^{87}Sr/^{86}Sr$	0·70359		0·70374	0·70354	0·70327	0·70355	0·70373	0·70414	0·70360
$^{143}Nd/^{144}Nd$	0·51290	0·51292	0·51289		0·51299	0·51289	0·51289	0·51280	0·51291

Sample no.	AGV−1	Deviation	BCR−2	Deviation	BHVO−1	Deviation	JA−2	Deviation	BR	Deviation
wt %										
SiO_2	59·06	0·26	54·53	0·78	49·81	0·31	56·05	0·16		
TiO_2	1·05	0·00	2·26	0·02	2·74	0·01	0·66	0·00		
Al_2O_3	17·09	0·08	13·61	0·28	13·65	0·11	15·44	0·10		
Fe_2O_3	6·72	0·03	13·80	0·15	12·16	0·12	6·25	0·03		
MnO	0·10	0·00	0·19	0·00	0·17	0·00	0·11	0·00		
MgO	1·53	0·01	3·67	0·07	7·20	0·08	7·91	0·07		
CaO	4·87	0·04	7·10	0·04	11·39	0·04	6·32	0·03		
Na_2O	4·26	0·10	3·29	0·15	2·37	0·12	3·07	0·08		
K_2O	2·93	0·00	1·79	0·02	0·53	0·01	1·75	0·01		
P_2O_5	0·50	0·00	0·37	0·01	0·28	0·01	0·15	0·00		
LOI	0·00		0·00							
Total	98·11		100·61		100·33		97·72			

Table 1: continued

Trace element deviation (ICP-MS) of measured standards from published values of Govindaraju (1995)

Sample no.	AGV–1	Deviation	BCR–2	Deviation	BHVO–1	Deviation	JA–2	Deviation	BR	Deviation
(ppm)										
Sc	11.7	0.31			30.4	1.03	18.2	1.03	19.3	4.02
V	130	6.82			298	13.6	134	6.68	213	15.6
Cr*	9.12				276	9.15	442	16.1	358	15.2
Co	14.6	0.45			42.9	1.49	27.5	1.74	53.6	1.17
Ni*	14.2	1.30			111	7.29	130	8.19	240	13.8
Cu	53.5	4.58			130		26.8		65.2	
Zn*	84.3	2.63			102	2.00	58.3	3.11	155	3.88
Mo	2.06	0.45			107	0.04	0.53	0.01	2.20	0.14
Rb	66.6	0.49			9.32	1.19	67.5	0.34	44.0	2.14
Sr	678	11.2			420	11.7	245	4.79	1129	135
Y	18.0	1.41			25.1	1.77	15.4	1.92	27.2	1.99
Zr	220	4.64			170	6.10	102	11.8	281	14.7
Nb	13.4	1.11			18.0	0.66	8.47	0.94	110	8.14
Cs	120	0.05			0.09	0.03	4.39	0.13	0.63	
Ba	1226				137		304	9.27	1077	19.5
La	37.9	0.04			15.7	0.03	15.0	0.89	80.9	0.79
Ce	69.0	1.43			39.4	0.28	31.6		150	0.45
Pr	8.35	0.53			5.55	0.10	3.54	0.59	16.9	0.06
Nd	31.6	0.96			25.4	0.12	13.7	0.02	64.4	0.42
Sm	5.84	0.04			6.37	0.13	2.95	0.12	11.9	0.23
Eu	1.58	0.04			2.12	0.04	0.85	0.06	3.50	0.14
Gd	4.78	0.15			6.36	0.03	2.91	0.14	9.63	0.10
Tb	0.66	0.02			0.99	0.02	0.47	0.04	1.27	0.01
Dy	3.62	0.02			5.55	0.25	2.86	0.10	6.22	0.12
Ho	0.69	0.02			1.04	0.04	0.58	0.09	1.05	0.03
Er	1.87	0.12			2.62	0.16	1.69	0.23	2.50	0.00
Tm	0.25	0.06			0.34	0.01	0.24	0.04	0.30	0.00
Yb	1.66	0.04			2.11	0.07	1.65	0.01	1.77	0.02
Lu	0.24	0.02			0.28	0.00	0.24	0.02	0.23	0.01
Hf	5.33	0.17			4.92	0.38	2.92	0.02	5.92	0.23
Ta	0.86	0.03			1.22	0.09	0.65	0.03	5.61	0.41
Pb	34.3	1.27			1.92	0.01	17.3	1.38	4.43	0.40
Th	6.44	0.04			1.32	0.18	4.77	0.05	10.5	0.35
U	1.90	0.01			0.43	0.01	2.11	0.20	2.49	0.00

A full dataset is available for downloading from http://www.petrology.oxfordjournals.org. The whole-rock (WR) major element data were determined by XRF and the trace element data by ICP-MS.

Spectrometer (ICP-MS) at the Institut für Geowissenschaften, University of Kiel. The samples were prepared following the pressurized $HF-HClO_4$–aqua regia acid digestion procedure described by Garbe-Schönberg (1993). Trace element analyses of the samples are given in Table 1; the standard deviation of the precision and accuracy is <5 and <8%, respectively, compared with the published data of Govindaraju (1995).

Mineral chemistry

Representative samples from Sete Cidades volcano were studied petrographically and mineral compositions were determined by electron microprobe. Major element analyses of glasses (Table 2) and minerals were carried out on a JEOL 8900 Superprobe electron microprobe at the Institut für Geowissenschaften, University of Kiel. The concentrations of the major elements as well as Cr_2O_3 and, in some cases, also Cl and NiO were measured. The machine was operated at an accelerating voltage of 15 kV, a beam current of 15 nA, using a focused beam with a diameter of 1 μm for minerals, and with a beam diameter of 12 μm for glasses. Counting times were set to 20 and 10 s for glasses $(Na_2O = 10/5$ s; $Cl = 120/60$ s; $Ni = 40/15$ s) and 15 and 7 s for mineral peaks and backgrounds, respectively.

Nd–Sr isotopes

The Nd and Sr isotopic compositions of most samples were determined at the Zentrallaboratorium für Geochronologie in Münster using a VG Sector 54 multicollector mass spectrometer. A few samples were analysed in static mode at the IFM–GEOMAR Research Centre in Kiel on a Finnigan MAT 262 RPQ2+ and on a Finnigan Triton mass spectrometer. For isotopic determinations, 100 mg of powdered sample material and standard ion exchange techniques (Hoernle *et al.*, 1991) were used to separate Sr and Nd from the matrix. The samples were leached for 1 h in hot ultrapure 6N HCl before dissolution. Procedural blanks in both laboratories were generally better than 0·2 ng for Sr and 0·1 ng for Nd. Sr isotope ratios were analysed in dynamic mode and isotope fractionation corrections made using $^{86}Sr/^{88}Sr = 0.1194$. In Münster, standard runs for Sr isotopes gave NBS 987 ($n = 16$): 0·710299 (2SD = 0·000026). Repeated measurement ($n = 12$) of the LaJolla Nd isotope standard yielded 0·511870 (2SD = 0·000018). In Kiel, the NBS987 ($n = 8$) gave 0·710273 (2SD = 0·000005) and the La Jolla standard yielded 0·511848 (2SD = 0·0000007). All Sr isotope analyses were normalized to NBS987 = 0·710250 and all Nd data are relative to a La Jolla of 0·511855.

PETROLOGY AND MINERAL CHEMISTRY

Petrology

The sampled rocks from all three different stratigraphic units range in composition from alkali basalt to trachyte based on the Total Alkalis vs SiO_2 (TAS) classification (Fig. 4) of Le Maitre *et al.* (1989). No major compositional gap or bimodality is observed; instead, all the samples lie along a well defined and relatively tight trend in the TAS diagram.

Primitive rocks

The mafic rocks of Sete Cidades can be classified as alkali-basalts (Fig. 4) with MgO contents between 14 and 5 wt %. Generally, the lavas from the post-caldera stage on Sete Cidades are more primitive than the pre-caldera lavas. The mafic rocks contain both olivine and clinopyroxene and smaller plagioclase phenocrysts in a fine-grained, often glassy matrix. The olivine and clinopyroxene phenocrysts are chemically and optically zoned. The high MgO samples (>12 wt % MgO, e.g. sample SM0101 in Tables 1, 2 and 3) show clear optical (xenomorphic shape) and chemical (disequilibrium) evidence for the accumulation of olivine and clinopyroxene xenocrysts. The olivine xenocrysts have corroded cores and are overgrown by clinopyroxene (Fig. 5a; Table 3). The mafic lavas from the young eruptive centres (e.g. Mafra, Ponta da Ferraria; Fig. 1) frequently contain xenoliths of peridotite, gabbro and syenite which show evidence of partial fusion.

Intermediate rocks

The intermediate rocks from Sete Cidades range from 2 to 5 wt % MgO and are classified as trachybasalt to trachyandesite (Fig. 4). Many of these rocks exposed at the coastline are slightly altered by sea-water (e.g. south of Mosteiros). Most intermediate rocks contain phenocrysts of olivine, clinopyroxene, plagioclase, titanomagnetite, ilmenite and apatite (Table 3). The olivines often have strongly iddingsitized and corroded rims, and altered cracks filled with red iron oxides and hydroxides. In contrast to the primitive basalts, the more evolved rocks contain up to 30% feldspar laths and up to 3% magnetite in the matrix (Table 3).

Evolved rocks (trachytes)

The trachytic lavas of Sete Cidades are mainly exposed on the inner caldera wall, at young eruption centres within the caldera, and at a trachytic dome located on the coast south of Mosteiros (Fig. 2). The trachytes have MgO contents of less than 2 wt % (Fig. 4; Table 1) and contain plagioclase and alkali feldspar pheno- and

Table 2: Major element and trace element compositions of glass samples from Sete Cidades

Sample no.	SM0103	SM0123	SM0143	SM9701	513DS—3	513DS—6	SM0101	SM0102	SM0131
Location	NW-cald wall	W-cald. wall	W-cald. wall	Miradoro do Carvao	W-flank Sete Cidades	W-flank Sete Cidades	Mafra flank vent	Mafra flank vent	Mafra flank vent
Long. (°N)	37.523	37.524	37.524	37.750	37.866	37.866	37.539	37.540	37.533
Lat. (°W)	25.474	25.486	25.486	25.710	25.938	25.938	25.490	25.492	25.483
Volcanic stage	pre-caldera stage	caldera-related deposit	caldera-related deposit	post-caldera stage	post-caldera stage	post-caldera stage	post-caldera stage	post-caldera stage	post-caldera stage
TAS classification	Trachyte	Trachyte	Trachyte	Basalt	Basalt	Basalt	Basalt	Basalt	Trachyandesite
(wt %)									
SiO_2	64.93	61.20	62.92	47.10	48.39	47.92	46.73	47.26	56.69
TiO_2	0.59	0.77	0.76	3.86	3.22	4.33	4.22	3.62	0.35
Al_2O_3	17.69	17.72	18.34	14.66	15.41	14.45	15.17	13.75	25.97
FeO^T	2.88	3.35	3.11	10.66	10.22	12.93	11.41	10.57	0.97
MnO	0.21	0.15	0.14	0.15	0.19	0.20	0.17	0.18	0.05
MgO	0.33	0.60	0.60	5.66	5.97	4.02	5.42	6.46	0.20
CaO	0.62	1.49	1.60	12.12	11.98	8.74	11.85	12.91	8.07
Na_2O	6.78	5.65	6.22	2.62	3.16	2.95	2.72	2.35	4.87
K_2O	5.71	5.97	5.71	1.57	1.58	2.45	1.95	1.75	2.70
P_2O_5	0.08	0.19	0.17	0.51	0.48		0.84	0.68	0.10
SO_3	0.01	0.02	0.02	0.05			0.03	0.01	0.01
F				0.32					
Cl	0.23	0.27	0.29	0.09			0.05	0.05	0.02
	12.49	11.62	11.93	4.19	4.74	5.40	4.67	4.10	7.57
Total	100.06	97.37	99.88	99.37	100.59	97.98	100.56	99.59	100.00
(ppm)									
Sc				26.4					
V									
Cr				330					
Co				43.4					
Ni				116					
Cu				89.8					
Mo				2.00					
Rb				29.8					
Sr				660					
Y				21.6					

Sample no.	SM0103	SM0123	SM0143	SM9701	513DS−3	513DS−6	SM0101	SM0102	SM0131
Location	NW-cald wall	W-cald. wall	W-cald. wall	Miradoro do Carvao	W-flank Sete Cidades	W-flank Sete Cidades	Mafra flank vent	Mafra flank vent	Mafra flank vent
Long. (°N)	37·523	37·524	37·524	37·750	37·866	37·866	37·539	37·540	37·533
Lat. (°W)	25·474	25·486	25·486	25·710	25·938	25·938	25·490	25·492	25·483
Volcanic stage	pre-caldera stage	caldera-related deposit	caldera-related deposit	post-caldera stage	post-caldera stage	post-caldera stage	post-caldera stage	post-caldera stage	post-caldera stage
Zr				206					
Nb				48·4					
Cs				0·35					
Ba				442					
La				38·6					
Ce				87·0					
Pr				10·2					
Nd				41·1					
Sm				8·73					
Eu				2·68					
Gd				7·44					
Tb				1·06					
Dy				5·72					
Ho				1·03					
Er				2·50					
Tm				0·32					
Yb				1·88					
Lu				0·27					
Hf				6·15					
Ta				3·28					
Pb				2·19					
Th				3·91					
U				1·19					

The major element compositions were determined by electron microprobe and the trace element data by ICP-MS.
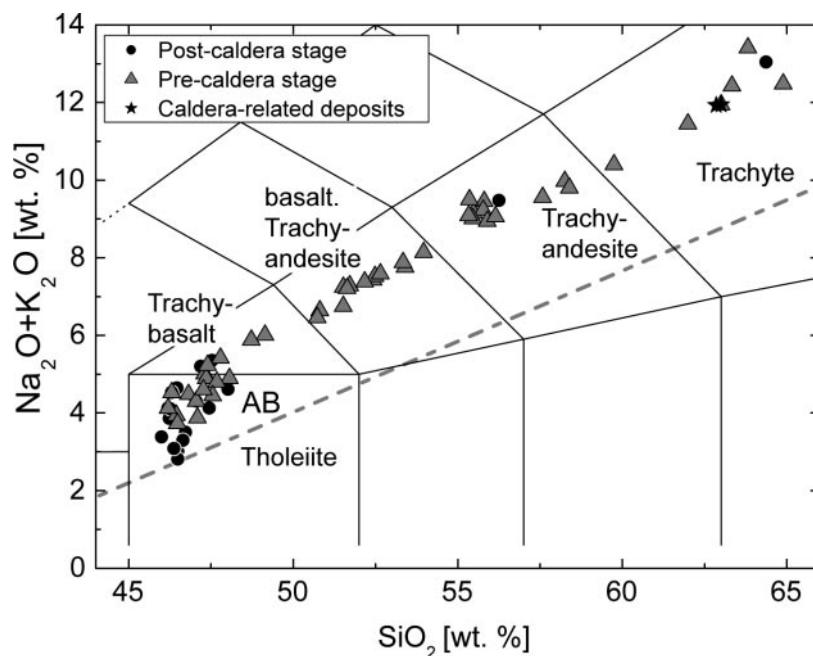
Fig. 4. Classification of the volcanic rocks of Sete Cidades according to the Total-Alkali versus SiO_2 diagram of Le Maitre et al. (1989). The dividing line between alkaline and tholeiitic compositions was taken from Macdonald (1968). All samples are in the range of the alkali-volcanic series. AB, alkali basalt.

xenocrysts, ilmenite and titanomagnetite and small amounts of kaersutite (Fig. 5b; Table 3). A few samples contain partly altered biotite crystals and strongly pleochroic aegirine-augite with highly corroded rims. The Sete Cidades volcano erupted a large volume of trachytic, partly glassy, pyroclastic air fall deposits. The matrix of these pyroclastic deposits consists of glassy, porous shards with plagioclase xenocrystals, and very small amounts of Ti-magnetite and ilmenite. The caldera outflow deposit consists of a fine-grained to glassy banded, porous matrix with olivine, pyroxene, plagioclase and kaersutite xenocrysts (Fig. 5c and d; Table 3). Other sections of these units consist of a volcaniclastic breccia, glass shards and xenocrysts, indicating an explosive eruptional event.

Mineral chemistry
Olivine

The analysed olivines range from Fo_{54-90} in the lavas of Sete Cidades with the higher Fo contents generally characteristic of phenocrysts and xenocrysts in the more mafic rocks. The olivine phenocrysts are normally zoned with a decreasing forsterite content from core to rim. The corroded olivine xenocrysts identified optically by their xenomorphic shape are chemically in disequilibrium with the surrounding glass matrix (Fig. 5a). Generally, the pre-caldera olivines have significantly lower Ni concentrations from 500 to 1500 ppm (Fo_{70-88}), whereas the post-caldera olivines have higher concentrations from 1000 to 2500 ppm (Fo_{88-89}). Primitive olivine phenocrysts cores (Fo_{89}) vary widely in their Ni concentrations, providing evidence for magma mixing processes. Forsteritic xenocrysts (Fo_{90}) were found in sample SM0140 from the Eguas eruption centre at the eastern flank of Sete Cidades (Fig. 1b).

Clinopyroxene

The Sete Cidades clinopyroxenes show moderate variations between $Wo_{39-46}En_{21-44}Fs_{17-29}$ and $Wo_{47-49}En_{37-48}Fs_{5-13}$. The majority of the clinopyroxene phenocrysts are normally zoned with decreasing MgO contents from the core towards the rim. However, a few crystals found in the intermediate and evolved rocks are reversely zoned, with higher Mg-number in the rims relative to the cores. The Al_2O_3 and TiO_2 contents abruptly increase above En contents of $\sim$40 (Fig. 6). Augites in the trachytic rocks show the lowest concentrations of Al_2O_3 ($>$0·5 wt %) and TiO_2 ($>$0·25 wt %). In contrast to the other oxides, Al_2O_3 and TiO_2 show a bimodality, with the basaltic rocks having the higher contents. The change in whole-rock compositions from basalt to trachyte is thus accompanied by a sharp decrease in Al_2O_3 and TiO_2 in the pyroxenes, rather than a continuous trend as formerly described by Renzulli & Santi (2000). As observed by Thompson (1974), the proportions of Al_{tot} and ^{VI}Al are positively correlated with the crystallization pressure of pyroxenes. The clinopyroxenes in

Table 3: Descriptions of sample localities and the petrology of representative samples

Sample no.	Location name:	Rock type	Description of petrology:
Pre-caldera stage:			
SM0103	NW-caldera wall Lagoa Azul	Trachyte	Fresh, fine-grained trachyte with glass, ∼3% Pl xenocrysts up to 4 mm, ∼3% Fe−Ti oxides xeno- and phenocrysts (<0·5 mm), 1% Cpx xenocrysts (<1 mm), <0·5% Bt phenocrysts (<0·5 mm)
SM0106	N-caldera wall Lagoa Azul	Trachyte	Fine to coarse grained trachyte, ∼50% Pl phenocrysts up to 1 mm, ∼3% Pl xenocrysts up to 3 mm, <1% Kaer xenocrysts (<1 mm), <0·5% Bt xenocrysts (<0·5 mm), sample contains a large accumulation of coarse grained (<5 mm) Pl (∼80%), Cpx (10%), and Fe−Ti oxide (∼10%) xenocrysts
SM0108	N-caldera wall, Lagoa Azul, E of SM0106	Basalt	Fine-grained basalt, ∼10% Pl phenocrysts up to 0·5 mm, ∼5% Cpx xenocrysts up to 2 mm, ∼3% Ol with corroded rims, very fine-grained Fe−Ti oxides in matrix, ∼0·5% Kaer (<1 mm) xenocrysts, resorbed Fe- oxide rims
SM0111	Coastline at Mosteiros	Basaltic trachyandesite	Fine-grained intermediate composition with 10% Pl xenocrysts (<3 mm), fine-grained Fe−Ti oxides and Pl phenocrysts in matrix (<0·2 mm)
SM0137	Ponta da Ferraria	Trachybasalt	Fine-grained Trachybasalt, ∼40% Pl phenocrysts (<0·5 mm), 7% sieve textured Pl xenocrysts (<1 mm), 3% Cpx and Ol xenocrysts (<1 mm), 1% Kaer phenocrysts (<4 mm) with a 100−200 μm opacitized reaction rim with Fe−Ti oxides, Pl and Cpx (∼1−5 mm)
SM0149	Relva Velha, S of Mosteiros	Trachyte	Fine-grained trachyte, 10% Pl phenocrysts (<2 mm), 5% of Fe−Ti oxide pheno- and xenocrysts (<0·5 mm), 5% Pl xenocrysts (<1 mm)
SM0166	Coastline S of Mosteiros	Basaltic trachyandesite	Fine-grained intermediate rock, ∼30% Pl phenocrysts (<0·5 mm), 1% Cpx xenocrysts (<0·5 mm)
SM0176	Coastline S of Mosteiros	Basaltic trachyandesite	Fine-grained intermediate composition, ∼5% Pl phenocrysts (<2 mm), ∼2% Fe−Ti oxide xenocrysts (<1 mm), matrix consists of fine-grained Fe−Ti oxides and Pl phenocrysts
SM 160501−1	W-caldera wall	Trachyandesite	Fine-grained porous evolved composition composition, 3% Pl phenocrysts (<0·5 mm), <1% Cpx xenocrysts (<0·5 mm)
Caldera related deposits:			
SM0123	NW-caldera rim	Trachyte	Fine-grained to glassy porous (∼15%) matrix with elongated glass shards (<20 mm), ∼2% Ol (<1 mm), ∼2% Cpx (<1 mm), 1−2% Pl (<1 mm), 0·5% Kaer (<2 mm) xenocrysts, <0·5% Bt xenocrysts (<5 mm)
SM0143	NW-caldera rim	Trachyte	Fine-grained matrix with elongated glass shards (<30 mm), 1% Ol (<1 mm), 1% Cpx (<1 mm), 1% Pl (<1 mm), <0·5% Bt xenocrysts (<0·5 mm)
Post-caldera stage:			
SM0101	Beira Mar de Beixo Coast at Mosteiros	Basalt	Fresh, fine-grained basalt with glass, ∼15% Ol and 10% Cpx phenocrysts (<4 mm), ∼5% Cpx and Ol xenocrysts, <1% Fe−Ti oxides (<0·5 mm)
SM0102	Beira Mar de Beixo Coast at Mosteiros	Basalt	Fresh, fine-grained basalt with glass, ∼10% Ol and 7% Cpx phenocrysts (<5 mm), ∼3% Cpx and Ol xenocrysts
SM0131	W-flank of Mafra	Basalt	Fine-grained basalt, 5% Cpx phenocrysts (<10 mm), 5% Ol (<2 mm), 3% Pl (<1 mm) xenocrysts
SM0140	Eguas flank vent E-flank of Sete Cidades	Basalt	Fine-grained basalt, ∼5% Cpx and 5% Ol phenocrysts (<2 mm) 2% Cpx and Ol xenocrysts (<3 mm)
SM0161	WSW- flank of Mafra vent	Basalt	Fine-grained basalt, 12% Cpx, 8% Ol phenocrysts (<1 mm), contains a cumulate with 75% Cpx, 15% Ol, 10% Pl (∼3 mm)
SM 220501−1	N of Ginetes, W-flank of Sete Cidades	Trachyte	Fine-grained to glassy trachyte, 7% Pl xenocrysts (<1·5 mm), 3% Fe−Ti oxide xenocrysts (<0·5 mm), <1% Cpx xenocrysts (<1 mm)
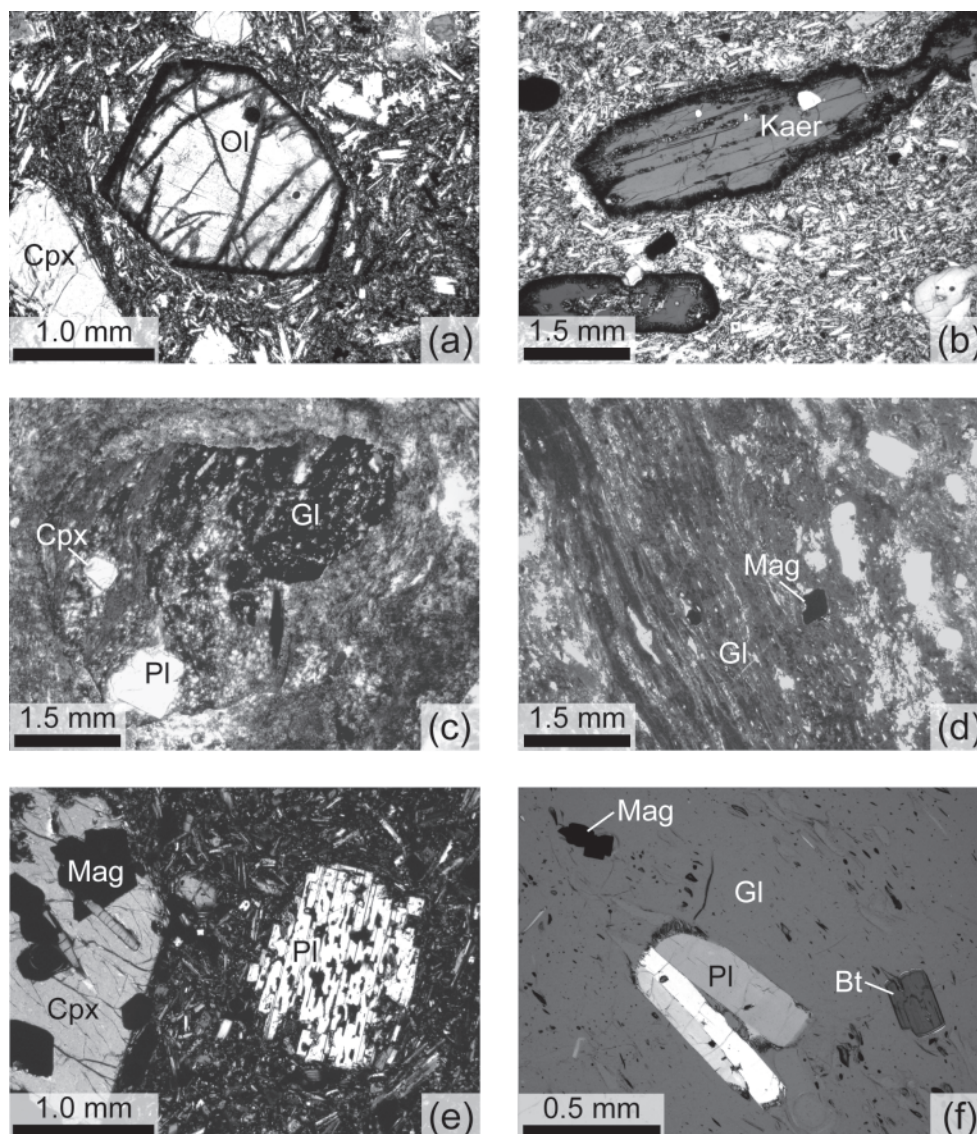
Fig. 5. Photomicrographs of representative thin sections of the Sete Cidades lavas. (a) Corroded olivine in sample SM0108; (b) Kaersutite (Kaer) phenocrysts with decompression rims in sample SM0137; (c) and (d) caldera-related outflow deposits (SM0123, SM0143) showing streaky glass shards (Gl) and plagioclase (Pl) and clinopyroxene (Cpx) xenocrysts as described in Table 3; (e) sieve textured plagioclase crystal in sample SM0137 under crossed polars; (f) plagioclase, magnetite and biotite crystals in sample SM0103 in a glassy matrix under half-crossed polars.

the trachytic samples have both lower Al_{tot} and lower ^{VI}Al than the clinopyroxenes in the basaltic samples. Therefore, two different pressure conditions can be inferred: (1) higher pressure conditions for the mafic rocks; and (2) shallower level conditions for the more evolved rocks (Pichavant *et al.*, 2002). As the proportion of Na_2O and Fe^{3+} increase with decreasing En content from basalts to trachytes in the Sete Cidades samples, this substitution suggests a relatively high oxygen fugacity during fractional crystallization (Pemberton & Offler, 1985). An enrichment of Na_2O in pyroxenes has been attributed to changes of the $Al_2O_3^{liquid}$ activity and oxygen fugacity by Ewart (1981). However, his work focuses on Na-rich pyroxenes, whereas the Sete Cidades pyroxenes have much lower Na_2O concentrations (up to 1·21 wt % Na_2O), suggesting that the compositional change in the Sete Cidades clinopyroxenes probably reflects a pressure decrease in the more evolved lavas.

Feldspar

The feldspars in the basaltic rocks are microphenocrysts and phenocrysts with a compositional range from bytownite to labradorite ($Ab_{15-37}An_{59-85}Or_{0-12}$; Fig. 7). The plagioclase phenocrysts in the hawaiites generally
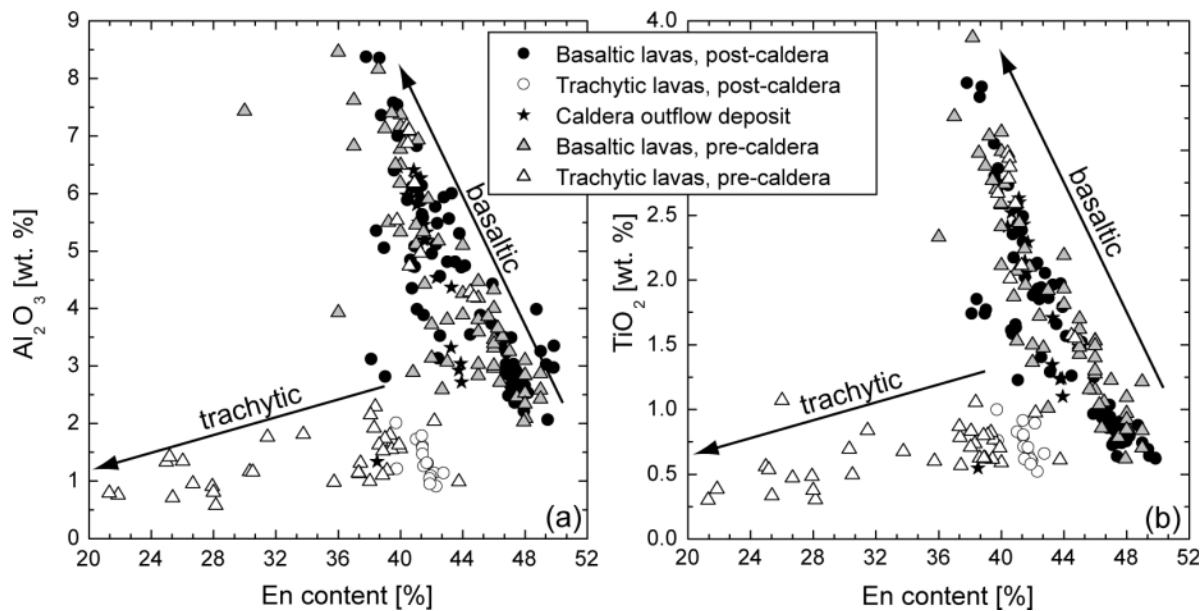
Fig. 6. Clinopyroxene compositions in lavas from Sete Cidades. (a) and (b) show the Al_2O_3 and TiO_2 (wt %) vs mole % En, respectively. Two trends can be distinguished: one having increasing Al_2O_3 and TiO_2 with decreasing En for the basaltic lavas and one with decreasing Al_2O_3 and TiO_2 for the trachytic lavas.
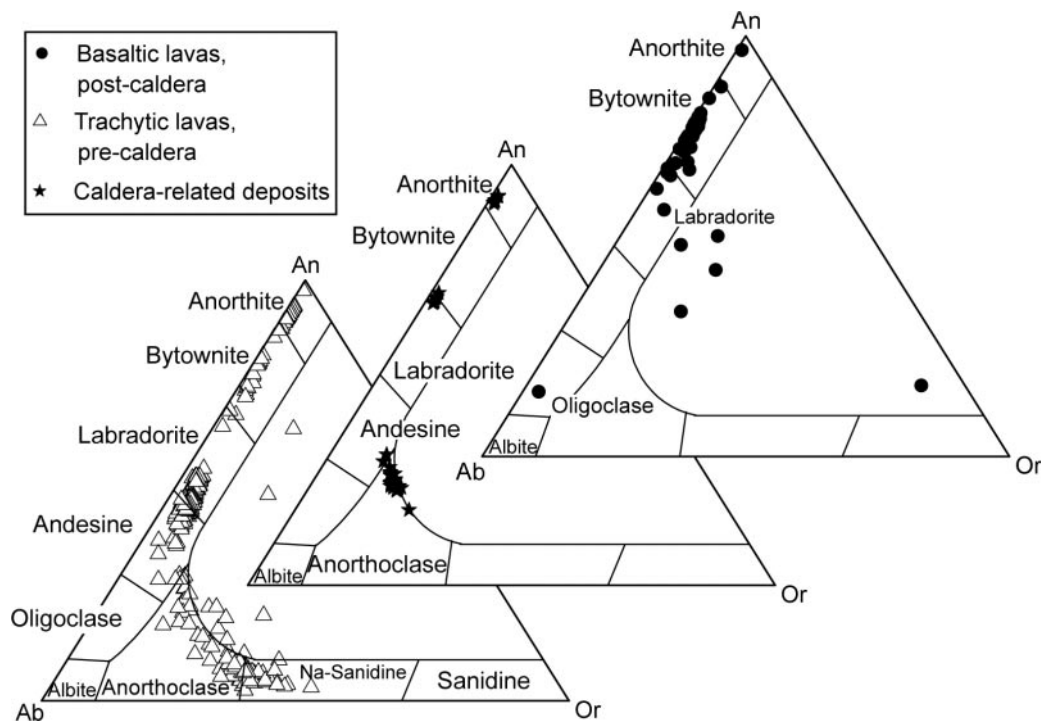
Fig. 7. Ternary feldspar compositions based on single spot electron microprobe analyses in the Sete Cidades lavas. The feldspars in the basaltic lavas (>5 wt % MgO) are relatively anorthite rich in contrast to the intermediate and trachytic samples (<5 wt % MgO) which cover a large range in the albite–anorthite fields. The feldspar xenocrysts in the caldera-related deposits show a bimodal distribution in the albite and anorthite fields.

show a relatively narrow range in the bytownite field ($Ab_{18-27}An_{67-82}Or_{0-6}$), with the higher albite contents reflecting fractional crystallization processes and decreasing CaO contents in the melt. The phenocrysts are typically weakly normally zoned. The mugearites show two compositional ranges in the anorthite (An_{86-93}) and bytownite (An_{64-82}) fields implying that the more anorthite-rich crystals likely derived from a more primitive magma. The feldspars in the trachytic rocks range from labradorite–andesine ($Ab_{42-60}An_{35-55}Or_{3-5}$) to anorthoclase–Na–sanidine ($Ab_{47-63}An_{3-22}Or_{14-50}$). The feldspar xenocrysts in sample SM0137 have disequilibrium textures that are commonly referred to as sieve-like textures (Fig. 5e), produced either by magma mixing or magmatic decompression (Nelson & Montana, 1992).

Spinel and iron–titanium oxides

Some basaltic and intermediate samples contain dark-brown Cr–spinel microphenocrysts. Microprobe analyses reveal that their chemical composition ranges from magnesiochromite to chromite (Table 4). The Cr–spinel occurs both as inclusions in olivine and clinopyroxene and in the matrix. The iron–titanium oxides in the Sete Cidades rocks are titanomagnetite in the basaltic and intermediate rocks, whereas ilmenite dominates over titanomagnetite in the more evolved rocks (trachytes and trachyandesites). The oxides can be found both as inclusions in phenocrysts and in the matrix. Some samples show a very dark tachylitic matrix as a result of presence of very fine-grained titanomagnetite crystals.

Amphibole

The intermediate (hawaiitic) and trachytic rocks contain abundant amphibole phenocrysts; amphibole xenocrysts occur rarely in the basaltic lavas (Fig. 5b). As the content of TiO_2 is approximately 7 wt % (e.g. SM0108; Table 4), the amphiboles are classified as kaersutites. The crystals are not zoned and have wide opacitized rims (SM0137) that are either associated with dehydration or pressure decrease as a result of magma ascent or with re-heating of the magma above the stability field of hornblende as a result of magma replenishment (Rutherford & Devine, 1988; Rutherford & Hill, 1993; Nicholis & Rutherford, 2004). Electron backscatter images from the EMP indicate the formation of new phases (1–5 μm) such as Fe–Ti oxides, plagioclase and Ca-rich clinopyroxene (diopside–hedenbergite), the two latter minerals confirmed by increasing CaO contents towards the rim of the kaersutites. The occurrence of Ca-rich clinopyroxene combined with a relatively thick rim (>100 μm) could provide evidence that some of these rims may have been generated by an 'overheating' of the magma in the stability field of Ca-rich clinopyroxene (855 °C, 0·13 GPa, Rutherford & Devine, 2003). However, the occurrence of sieve-textured, normally zoned, plagioclase

xenocrysts and mostly normally zoned clinopyroxene xenocrysts in this sample rather suggest decompression processes. Some amphibole phenocrysts show strongly resorbed rims with abundant iron oxides, especially in sample SM0108.

Biotite

Biotite crystals were only observed in the trachytic rocks (Fig. 5f; Table 3). They occur as greenish-brown strongly pleochroic phenocrysts of phlogopite to biotite with a substitution of K_2O by small amounts of Na_2O. According to Burnham (1979) and Wones & Gilbert (1982), crystallization processes in alkaline magmas are sensitive to water pressure and oxygen fugacity. Amphibole crystallizes earlier than biotite at higher pressures; for example, at 750 °C, amphibole crystallizes between 1 and 2 kbar, whereas biotite crystallizes at pressures ≪1 kbar (Wones & Gilbert, 1982). The stability of micas is greatly enhanced by lowered SiO_2 activities. The restricted occurrence of biotite in the Sete Cidades trachytic samples suggests that the SiO_2 activity was relatively low; this is confirmed by the absence of quartz in the Sete Cidades lavas. Thus, the trachyte magmas of Sete Cidades are inferred to have had a relatively high water pressure and oxygen fugacity at low SiO_2 activities in order to crystallize amphibole before biotite.

Apatite

Small (<1 mm) idiomorphic to hypidiomorphic apatite crystals occur in the matrix and as inclusions in clinopyroxene phenocrysts in the intermediate rocks (1–3% MgO), and in mafic and ultramafic xenoliths. The apatite inclusions in the xenoliths are Cl–F apatites (Hansteen, unpublished data), indicating relatively high halogen activities in the crustal magma reservoirs.

Geochemistry

Whole-rock compositions

With decreasing MgO, SiO_2, Na_2O and K_2O show slight increases of between 4 and 6 wt % MgO, but then very abruptly increase in abundance at lower MgO contents (Fig. 8). The concentrations of Al_2O_3 and P_2O_5 reach a maximum at 1·5 and 3 wt % MgO, respectively, and then decrease, whereas TiO_2 and FeO^T increase to ~5 wt % MgO and then decrease steeply (Fig. 8). Lavas with more than 4 wt % MgO show a positive correlation between MgO and Ni concentrations (Fig. 9a); lavas from the Mafra flank eruption show a coherent linear trend extending to high Ni and MgO contents (Fig. 9b).

The Sete Cidades pre-and post-caldera lavas are characterized by very similar incompatible element ratios, with the exception of $(La/Sm)_N$, Ba/Nb and La/Nb, which are lower [$(La/Sm)_N$] and higher (Ba/Nb, La/Nb) in the post-caldera lavas than in the older series

Table 4: Representative mineral compositions determined by electron microprobe. Fe_2O_3 calculated assuming stoichiometry; Fe_2O_3 for amphiboles after Droop (1987)

Sample	SM0101	SM0140	SM0140	SM0133	SM0136	SM0101	SM0102	SM0103	SM0108	SM0108	SM0108	SM0108	SM0123	SM0123	SM0123
Volcanic stage	post-caldera	post-caldera	post-caldera	pre-caldera	pre-caldera	post-caldera	post-caldera	pre-caldera	pre-caldera	pre-caldera	pre-caldera	pre-caldera	caldera-related	caldera-related	caldera-related
Mineral	Ol	Ol	Ol	Ol	Ol	Cpx	Cpx	Cpx	Cpx	Cpx	Cpx	Cpx	Cpx	Cpx	Cpx
	core	core	rim	core	core	core	rim	core	core	core	rim	core matrix	rim	core	core
Total no. of analyses per sample	25 ss	34 ss		29 ss	36 ss	15 ss	7 ss, 1 profile	8 ss	14 ss				15 ss		
SiO_2	40·44	40·66	40·32	39·16	39·34	52·26	52·22	52·59	53·00	52·03	49·15	51·05	47·88	46·99	48·88
TiO_2						0·84	0·64	0·53	0·86	0·88	1·72	1·87	2·43	2·76	2·14
Al_2O_3						2·21	2·65	0·88	2·09	2·97	5·17	2·89	5·92	6·46	5·19
Cr_2O_3						0·62	0·96	0·02	0·29	0·41	0·60	0·03	0·03	0·02	0·00
FeO	11·75	10·84	11·57	18·35	18·26	3·37	3·87	8·07	3·60	4·26	5·13	7·71	4·96	5·53	5·10
Fe_2O_3						0·38	0·00	2·07	0·00	0·00	0·63	0·13	2·40	2·81	2·27
MgO	47·32	47·97	47·57	42·00	41·69	16·71	16·24	12·17	16·89	16·18	14·13	13·67	13·57	12·90	13·83
MnO	0·22	0·18	0·18	0·30	0·32	0·12	0·11	1·45	0·06	0·11	0·04	0·21	0·16	0·19	0·20
CaO	0·28	0·30	0·27	0·26	0·33	22·37	21·95	20·72	22·60	22·11	22·23	21·48	21·87	21·62	22·19
Na_2O						0·28	0·36	1·21	0·20	0·29	0·32	0·61	0·46	0·48	0·43
K_2O											0·00	0·03	0·00	0·01	0·00
NiO	0·24	0·29	0·32	0·15	0·13	0·00	0·00	0·00	0·00	0·00			0·00	0·00	0·00
Total	100·25	100·25	100·24	100·21	100·07	99·15	99·01	99·71	99·59	99·25	99·11	99·68	99·67	99·76	100·24
Mg-number	89	90	90	83	83	89	90	86	89	89	82	76	80	77	80

Sample	SM0133	SM0137	SM0137	SM0140	SM0140	SM0143	SM0143	SM220501−1	SM0166	SM160501−4	SM160501−4	SM0106	SM0108	SM0123
Volcanic stage	pre-caldera	pre-caldera	pre-caldera	post-caldera	post-caldera	caldera-related	caldera-related	post-caldera	pre-caldera	pre-caldera	pre-caldera	pre-caldera	pre-caldera	caldera-related deposit
Mineral	Cpx	Cpx	Cpx	Cpx	Cpx	Cpx	Cpx	Cpx	Cpx	Cpx	Cpx	Kaer	Kaer	Kaer
	core	rim	core	rim	core	rim	core	core xenocryst	core phenocryst	rim	core	core	core	core
Total no. of analyses per sample	15 ss, 7 profiles		24 ss		14 ss, 1 profile		5 ss	18 ss	7 ss		14 ss	5 ss	4 ss	13 ss
SiO_2	47·81	46·19	50·95	50·71	52·72	48·24	51·24	51·62	47·49	47·31	51·17	42·11	40·13	41·33
TiO_2	2·33	3·14	1·26	1·85	0·63	2·38	1·10	0·83	2·53	2·70	1·04	4·37	7·34	5·65
Al_2O_3	6·83	7·17	3·54	3·13	2·97	5·87	2·72	1·73	6·63	6·50	3·66	10·12	12·41	11·58
Cr_2O_3	0·38	0·27	0·10	0·03	0·39	0·20	0·00	0·00	0·06	0·18	1·03	0·00	0·08	0·00
FeO	5·16	4·98	5·39	7·01	4·06	5·23	5·22	6·70	5·38	5·49	3·90	0·43	6·03	11·02
Fe_2O_3	1·63	2·43	0·93	0·51	0·18	1·59	1·77	2·07	2·14	1·61	0·32	13·46	1·05	0·00
MgO	13·51	12·89	15·17	14·48	17·30	13·62	15·02	13·71	13·13	12·87	15·78	12·56	18·28	13·36
MnO	0·14	0·11	0·18	0·20	0·11	0·20	0·34	0·89	0·14	0·19	0·05	0·60	0·07	0·21
CaO	21·68	21·84	21·65	21·52	20·89	22·10	21·71	20·73	21·90	22·21	22·31	11·28	0·03	11·45

Table 4: continued

	SM0133	SM0137	SM0137	SM0137	SM0140	SM0143	SM0143	SM220501-1	SM0166	SM160501-4	SM160501-4	SM0106	SM0108	SM0123
Volcanic stage	pre-caldera	pre-caldera	pre-caldera	pre-caldera	post-caldera	caldera-related	caldera-related	post-caldera	pre-caldera	pre-caldera	pre-caldera	pre-caldera	pre-caldera	caldera-related deposit
Mineral	Cpx	Kaer	Cpx	Cpx	Cpx	Cpx	Cpx	Cpx	Cpx	Cpx	Cpx	Kaer	Kaer	Kaer
	core	core	core	rim	core	core	rim	core xenocryst	core phenocryst	core	rim	core	core	core
Total no. of analyses per sample	15 ss (7 profiles)		24 ss		14 ss (1 profile)	5 ss		18 ss	7 ss	14 ss		5 ss	4 ss	13 ss
Na$_2$O	0.46	0.43	0.37	0.37	0.39	0.45	0.39	0.84	0.45	0.32	0.42	2.75	0.89	2.63
K$_2$O	0.00	0.00	0.00	0.00	0.00	0.00	0.00	0.00	0.00	0.00	0.00	1.20	9.09	0.97
NiO	0.00	0.00						0.00		0.00	0.00	0.00	0.00	0.00
Total	99.92	99.45	99.54	99.81	99.65	99.58	99.82	99.10	99.84	99.56	99.48	98.87	95.38	98.20
Mg-number	81	79	82	78	88	82	80	77	74	87	79			

	SM0137	SM0137	SM0143	SM180501-1a	SM0103	SM0106	SM0123	SM0143	SM0101	SM0106	SM0108	SM0123
Volcanic stage	pre-caldera	pre-caldera	caldera-related	pre-caldera	pre-caldera	pre-caldera	caldera-related	caldera-related	post-caldera	pre-caldera	pre-caldera	caldera-related
Mineral	Kaer	Kaer	Kaer	Kaer	Bt	Bt	Bt	Bt	Chr	Mag	Mag	Mag
	core	rim	core	core	core	core	core	core	core	core	core	core
Total no. of analyses per sample	29 ss core-rim analyses		12 ss	10 ss	12 ss	15 ss	7 ss	16 ss	4 ss	25 ss	22 ss	9 ss
SiO$_2$	39.56	43.80	40.96	38.87	38.74	36.70	36.48	35.97	0.00	0.00	0.00	0.11
TiO$_2$	5.93	5.42	6.10	6.79	5.65	6.51	7.14	7.25	3.81	14.65	14.68	17.86
Al$_2$O$_3$	13.36	8.05	11.82	12.46	12.20	13.30	13.69	13.66	14.07	0.99	1.50	5.59
Cr$_2$O$_3$	0.00	0.00	0.00	0.04	0.00	0.00	0.03	0.00	36.20	0.02	0.00	0.06
FeO	0.38	6.92	0.81	13.01	15.00	9.01	15.98	10.76	18.51	39.25	39.50	37.73
Fe$_2$O$_3$	11.24	1.89	10.30	0.00	0.00	6.85	0.00	5.64	14.42	40.01	39.48	30.99
MgO	12.77	11.44	13.32	11.46	14.68	13.91	12.97	12.95	12.07	1.77	1.98	6.75
MnO	0.08	0.15	0.24	0.25	0.53	0.41	0.30	0.35	0.34	2.63	1.96	0.42
CaO	11.95	21.33	11.81	11.25	0.01	0.00	0.01	0.00	0.00	0.00	0.00	0.00
Na$_2$O	2.29	0.53	2.57	2.68	0.93	0.97	0.98	0.92	0.00	0.00	0.00	0.00
K$_2$O	1.14	0.00	0.99	0.94	8.98	8.71	8.50	8.69	0.00	0.00	0.00	0.00
NiO											0.01	0.08
ZnO											0.23	0.03
Total	98.70	99.53	98.92	97.75	96.72	96.37	96.08	96.19	99.42	99.32	99.35	99.61

Table (upper block)

	SM0137	SM0137	SM0140	SM0143	SM180501–1a	SM0140	SM0137	SM0123	SM0106		SM0123	SM0137	SM0103
Sample	SM0137		SM0140	SM0143	SM180501–1a	SM0140	SM0137	SM0123	SM0106		SM0123	SM0137	SM0103
Volcanic stage	pre-caldera		post-caldera	caldera-related	pre-caldera	post-caldera	pre-caldera	caldera-related	pre-caldera		caldera-caldera	pre-caldera	pre-caldera
Mineral	Mag		Mag	Mag	Mag	Mag–Chr	Ti–Mag	Ti–Mag	Ilm		Ilm	Ilm	Pl
	core	rim	core	core	core	core	core	core	core	core	core	core	core
Total no. of analyses per sample	38 ss		6 ss	11 ss	17 ss	14 ss	2 ss	1 ss	4 ss		6 ss	5 ss	6 ss
SiO_2	0·00	0·00	0·00	0·00	0·10	0·00	0·00	0·08	0·00	0·00	0·05	0·00	66·29
TiO_2	14·93	17·73	16·77	17·12	18·35	2·90	20·47	29·68	46·94	45·93	49·82	46·42	0·00
Al_2O_3	5·48	4·93	4·85	1·65	3·01	14·81	4·39	1·53	0·05	0·10	0·17	0·48	19·36
Cr_2O_3	0·00	0·00	0·00	0·00	0·00	37·75	0·00	0·00	0·01	0·00	0·00	0·00	0·00
FeO	37·71	40·41	39·52	42·14	42·68	14·57	42·36	55·08	36·60	36·39	36·76	30·01	0·30
Fe_2O_3	35·85	30·32	32·64	34·48	29·47	12·38	26·61	7·09	10·63	12·48	6·17	15·42	0·00
MgO	4·90	4·59	4·58	2·07	2·20	13·50	4·99	1·11	1·38	1·04	3·37	6·31	0·00
MnO	0·40	0·42	0·58	1·63	1·76	0·33	0·52	0·66	2·99	2·95	1·96	0·44	0·00
CaO	0·00	0·00	0·00	0·00	0·00	0·00	0·00	0·00	0·00	0·00	0·00	0·00	0·45
Na_2O	0·00	0·00	0·00	0·00	0·00	0·00	0·00	0·00	0·00	0·00	0·00	0·00	7·02
K_2O	0·00	0·00	0·00	0·00	0·00	0·00	0·00	0·00	0·00	0·00	0·00	0·00	6·55
NiO					0·03			0·03	0·06	0·00			
ZnO					0·26	0·11	0·13	0·09	0·10	0·11	0·13	0·06	
Total	99·27	98·40	98·94	99·08	97·87	96·35	99·48	95·34	98·75	99·00	98·43	99·15	99·98

Table (lower block)

	SM0106		SM0108	SM0108	SM0123	SM0136	SM0143	SM220501–1	SM0149		SM0166	SM180501–1a	
Sample	SM0106		SM0108	SM0108	SM0123	SM0136	SM0143	SM220501–1	SM0149		SM0166	SM180501–1a	
Volcanic stage	pre-caldera		pre-caldera	pre-caldera	caldera-caldera	pre-caldera	caldera-related	post-caldera	pre-caldera		pre-caldera	pre-caldera	
Mineral	Pl		Pl	Kfs	Pl	Pl	Pl	Pl	Pl		Pl	Pl	
	core	core	core matrix	core	core	core	core	core	core phenocryst	core	core	core	core
Total no. of analyses per sample	21 ss		12 ss	1 ss	19 ss	42 ss	17 ss	10 ss	61 ss		13 ss	13 ss	
								7 profiles					
SiO_2	63·68	66·08	51·68	61·16	46·88	51·29	63·91	64·12	60·20	66·31	54·71	62·98	47·50
TiO_2	0·00	0·00	0·00	0·27	0·00	0·00	0·00	0·76	0·00	0·02	0·00	0·00	0·00
Al_2O_3	21·87	19·90	31·08	17·37	34·44	30·25	21·65	17·20	24·70	18·80	29·28	22·42	33·53
Cr_2O_3	0·00	0·00	0·00	0·00	0·00	0·00	0·00	0·00	0·00	0·06	0·00	0·00	0·00
FeO	0·37	0·35	0·79	0·82	0·23	0·82	0·28	2·81	0·31	0·29	0·82	0·40	0·62
Fe_2O_3	0·00	0·00	0·00		0·35	0·00	0·00	0·00	0·00	0·00	0·00	0·00	0·00
MgO	0·00	0·00	0·00	3·99	0·00	0·00	0·00	0·51	0·00	0·02	0·00	0·00	0·00
MnO	0·00	0·00	0·00	0·05	0·00	0·00	0·00	0·22	0·00	0·00	0·00	0·00	0·00
CaO	2·42	0·80	12·33	1·62	16·83	13·25	2·69	0·93	6·25	0·48	10·30	3·38	16·41
Na_2O	7·58	6·76	4·24	0·87	1·70	3·50	7·62	7·02	7·08	6·36	4·83	7·79	1·90
K_2O	3·31	6·37	0·27	12·09	0·07	0·32	3·43	5·77	1·10	7·64	0·43	2·16	0·07
Total	99·23	100·26	100·39	98·24	100·51	99·43	99·58	99·46	99·64	99·98	100·37	99·13	100·02

Abbreviation ss indicates single spot analyses.
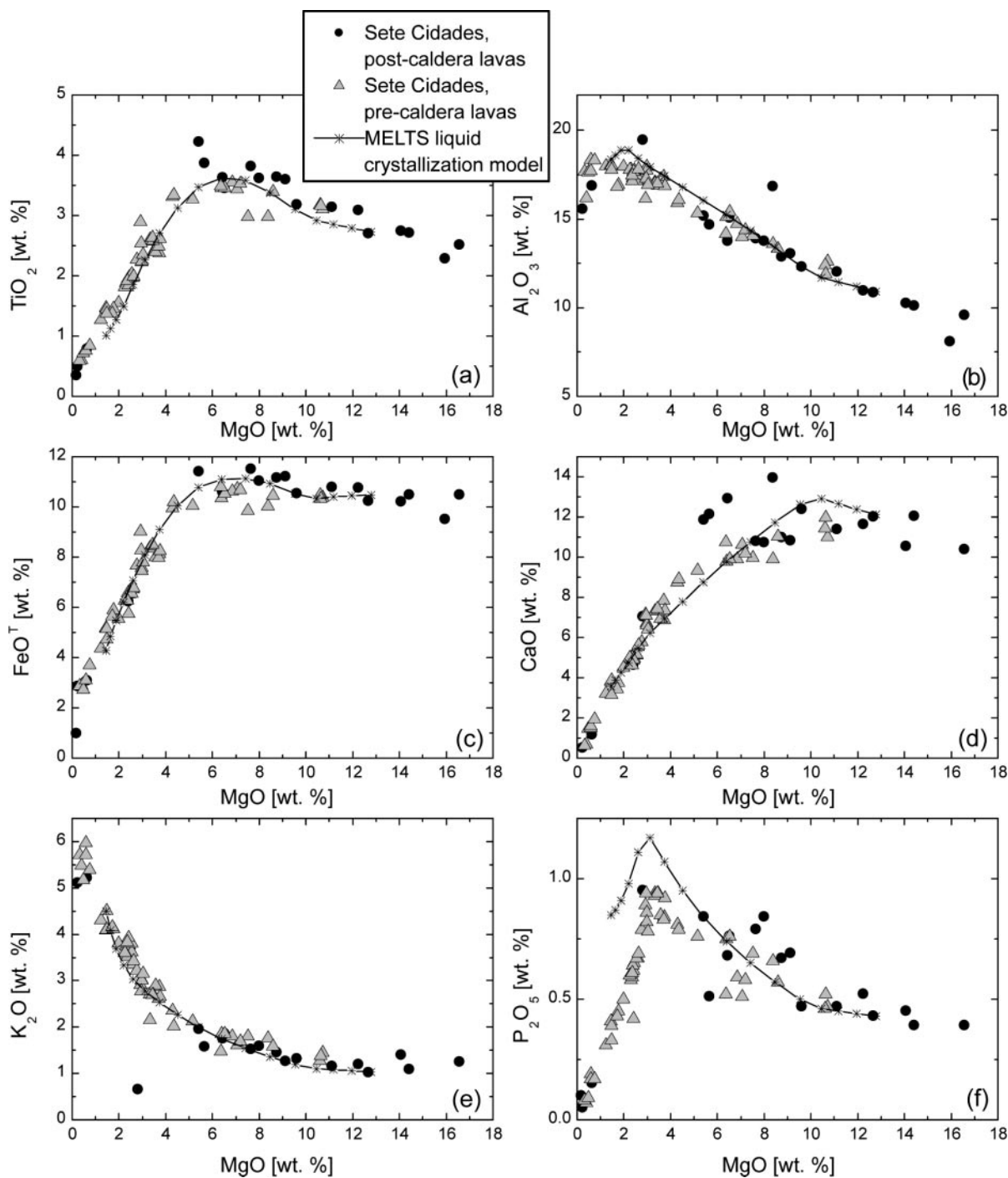
Fig. 8. Major element contents (a) TiO_2; (b) Al_2O_3; (c) FeO^T; (d) CaO; (e) K_2O; and (f) P_2O_5 plotted vs MgO contents for the Sete Cidades lavas. Lines indicate fractional crystallization trends modelled by MELTS (Ghiorso & Sack, 1993) using SM0140 as the parental magma, as discussed in the text. The tick marks on the model curves indicate temperature steps of 20 °C, starting at a temperature of 1311 °C and a pressure of 5 kbar.

at a given MgO content (Fig. 10). Whereas $(La/Sm)_N$, Nb/Ta and Zr/Hf show increasing concentrations with decreasing MgO contents, the Nb/Zr and Ba/Nb of the products of each volcanic stage remain constant over the range of MgO concentrations. La/Nb is constant

between 14 and 3 wt % MgO but decrease significantly at MgO contents lower than 3 wt %.

The lavas and glasses from Sete Cidades form a broad negative trend in $^{87}Sr/^{86}Sr$ versus $^{143}Nd/^{144}Nd$ extending to much higher $^{87}Sr/^{86}Sr$ and lower $^{143}Nd/^{144}Nd$
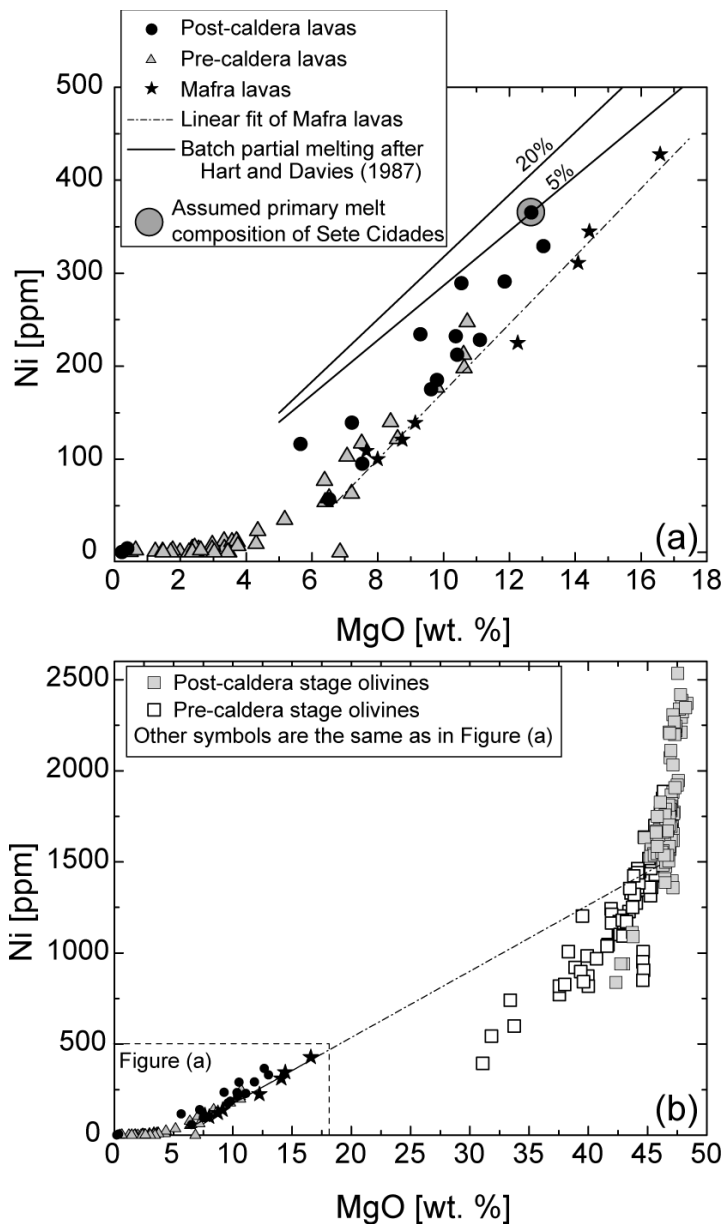
Fig. 9. (a) Variation of Ni [ppm] vs wt % MgO in the Sete Cidades lavas. Also shown is the range of primary magma compositions of Hart and Davies (1978) for 5 and 20% partial melting of a mantle peridotite; (b) lava compositions from (a) and single spot analyses of the Sete Cidades olivine phenocrysts. Dotted line indicates a mixing line between the Sete Cidades primitive basalts with olivine phenocrysts in the Mafra lavas.

isotope ratios than the range of previously published data (Fig. 11a). Lavas from the pre-caldera stage generally have lower Sr isotope ratios (<0·7036) than the post-caldera lavas (0·70355–0·70414), but there is a significant overlap. One sample of the post-caldera stage (SM0114) has a relatively high Sr isotope ratio of 0·70418 at a Nd isotope ratio of 0·51291, which is similar to the bulk of the Sete Cidades lavas. This radiogenic Sr isotope composition probably reflects sea-water alteration (O'Nions *et al.*, 1977; Whipkey *et al.*, 2000). However, all other samples from Sete Cidades show a coherent correlation between

Sr and Nd isotopic ratios, implying a source signature rather than sea-water alteration processes. Interestingly, the lavas from the Mafra eruption have extremely heterogeneous Sr–Nd isotope compositions ($^{87}Sr/^{86}Sr$: 0·7035–0·7042; Fig. 11a). Some literature data from the neighbouring Agua de Pau volcanic system are also plotted in Fig. 11. The Agua de Pau Sr and Nd isotope ratios extend towards 0·7055 and 0·5127, respectively (White *et al.*, 1979; Feraud *et al.*, 1980; White & Hofmann, 1982; Storey *et al.*, 1989; Turner *et al.*, 1997; Widom *et al.*, 1997). The Rb/Sr and Sr isotope ratios of
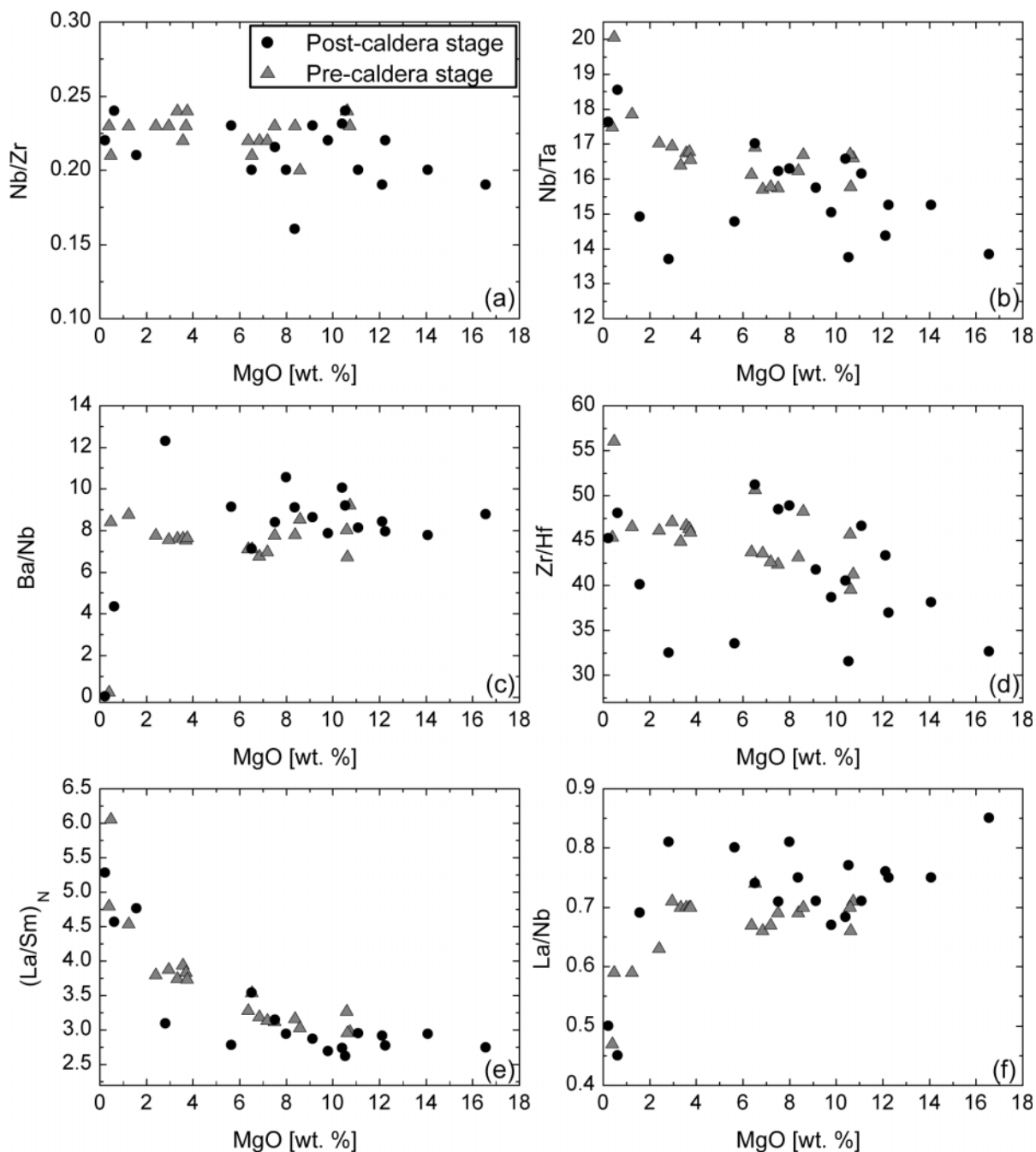
Fig. 10. Highly incompatible trace element ratios vs wt % MgO in the lavas from Sete Cidades.

the Sete Cidades and Agua de Pau samples show a broad positive correlation (Fig. 11b) with higher Rb/Sr and Sr isotope ratios at Agua de Pau. Three samples from the Mafra vent define a positive trend towards the fields of Agua de Pau samples.

Glasses

Glasses were found either as crusts on post-caldera flank deposits or in the post-caldera and caldera outflow

pyroclastic deposits. The major and trace element compositions of these glasses follow the trends observed in the whole-rock lava samples. Some of the most primitive lavas (SM0101 and SM0102) from the Mafra eruption have MgO whole-rock contents of 12·3 and 14·1 wt %. These lavas have associated glass crusts with MgO contents of 5·4 and 6·5 wt %, respectively, implying that the accumulation of olivine and clinopyroxene xenocrysts has modified the bulk-rock
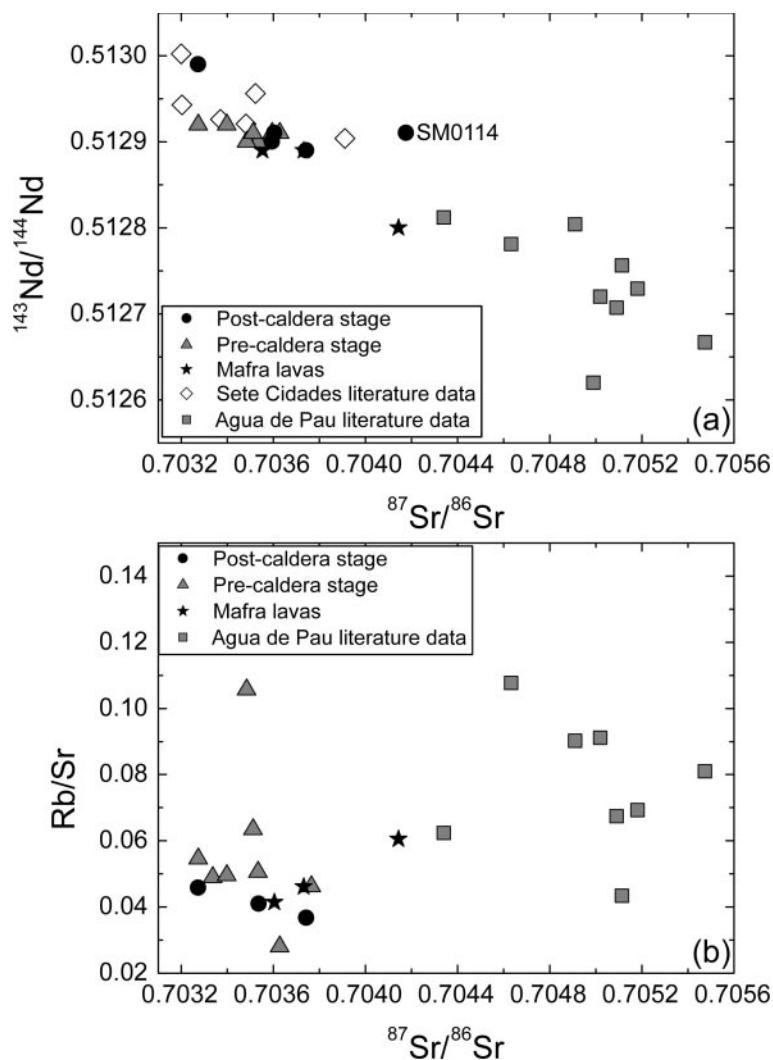
Fig. 11. (a) Variation of $^{87}Sr/^{86}Sr$ vs $^{143}Nd/^{144}Nd$ for the Sete Cidades lavas and Agua de Pau data from the literature (White *et al.*, 1979; Feraud *et al.*, 1980; White & Hofmann, 1982; Storey *et al.*, 1989; Turner *et al.*, 1997; Widom *et al.*, 1997). Literature data from Sete Cidades are also plotted for comparison (White *et al.*, 1975; Hawkesworth *et al.*, 1979; Davies *et al.*, 1989; Turner *et al.*, 1997; Widom *et al.*, 1997). (b) Rb/Sr vs $^{87}Sr/^{86}Sr$ for the Sete Cidades and Agua de Pau volcanic systems. Sources of data as in (a).

composition, as already suggested from petrological observations.

The caldera outflow deposit

Thick pyroclastic deposits, suggested to have erupted during caldera formation (Moore, 1990), contain abundant streaky glass shards of heterogeneous chemical compositions between 1·0 and 0·3 wt % MgO (Fig. 12). On major element diagrams, the compositions of larger glass shards lie along linear trends, suggesting mixing of two different liquids (Fig. 12). The trachytic glass SM0123 from the caldera outflow deposit has Mg-numbers of 19–33 but contains rare olivines with Fo_{81}, which would be in equilibrium with a liquid of Mg-number of ~50,

supporting mixing of a more primitive magma with an evolved magma composition. Two inversely zoned clinopyroxene xenocrysts have been found in sample SM0123, also providing evidence for magma mixing processes.

DISCUSSION
Primitive magmas of Sete Cidades and their formation

Primitive magmas from the mantle must be in equilibrium with olivine (Sato, 1977; Hart & Davis, 1978; Hess, 1992), and, thus, the MgO and Ni contents of the most primitive lavas and olivine phenocrysts among the Sete
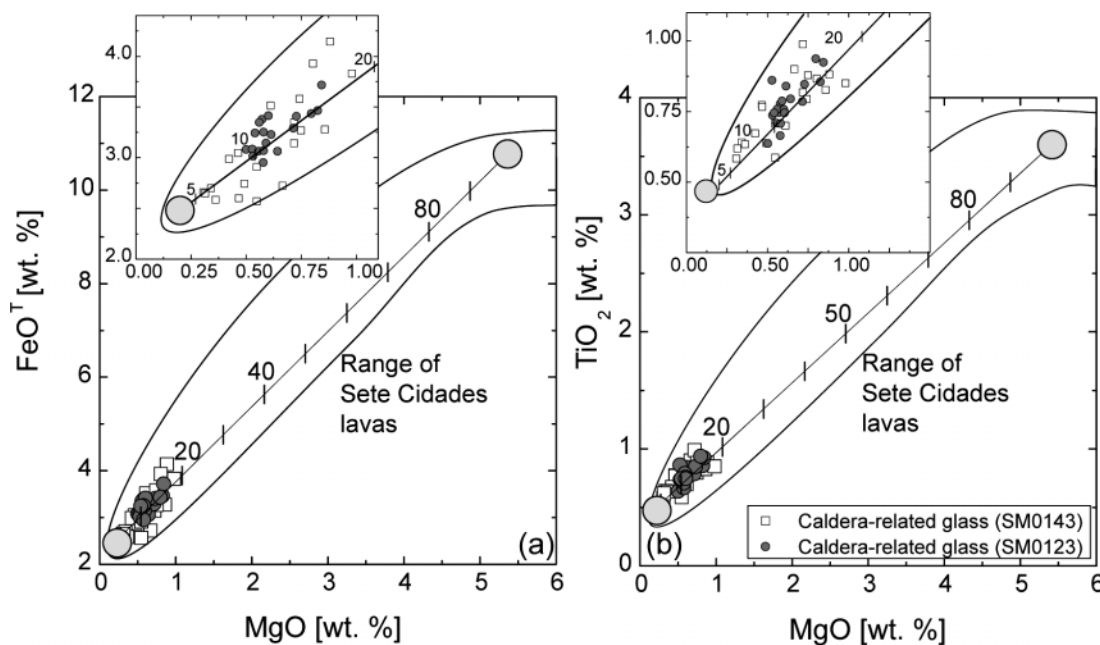
Fig. 12. Variation of (a) FeO^T and (b) TiO_2 vs MgO (wt %) in glass shards from two samples of the caldera-related pyroclastic deposit indicating strong heterogeneity within the glasses and possible mixing trends between intermediate and basaltic melt. Field shows the range of the Sete Cidades pre- and post-caldera lavas. The grey circles indicate the end-members of the mixing array. The basaltic magma MgO content has been estimated at about 5 wt % MgO based on olivine xenocrysts in the glasses of the caldera outflow deposit. The insets illustrate the variation of the caldera-related deposits in more detail.

Cidades volcanic rocks can be used to estimate the primary magma composition (Fig. 9). The most primitive glasses analysed from the Sete Cidades volcano have MgO contents of about 6·5 wt % and do not represent primary magma compositions. According to Hess (1992), a primary melt must have at least 10 wt % MgO and a Ni content of 400 ppm. The Sete Cidades sample SM0140 has a whole-rock MgO content of 12·7 wt % and a Ni content of 365 ppm, resembling a primary magma formed by 5% partial melting of a peridotite mantle source (Fig. 9) according to the model of Hart & Davis (1978). The olivines in SM0140 ($Fo_{88–89}$) are in equilibrium with the bulk-rock composition (Mg-number 70) using the olivine–liquid equilibrium of Roeder & Emslie (1970). Although this sample contains small amounts of xenomorphic olivine, the majority of the olivines are idiomorphic to hypidiomorphic, suggesting equilibrium crystallization from the magma. The analysed olivine phenocrysts are the most primitive from Sete Cidades, with a Ni concentration range of 1300–2500 ppm at $Fo_{88–90}$, suggesting that these olivines crystallized in equilibrium with a melt of similar composition to SM0140. Therefore, we conclude that sample SM0140 represents a near-primary melt composition of the Sete Cidades magma system. Concentrations of MgO higher than ~12 wt % are, thus, considered as a result of the accumulation of olivine and clinopyroxene, as these lavas contain abundant olivine and clinopyroxene xenocrysts

(Tables 1, 3 and 4). The range of chemical variation in the Sete Cidades volcanic rocks with MgO contents below 12 wt % is probably a result of fractional crystallization processes.

The primitive magmas of both the pre- and post-caldera stages are similar in terms of their major element compositions, ratios of the heavy rare earth elements, and also in most incompatible element ratios sensitive to the degree of partial melting (Figs 8 and 10). Consequently, the degree and the depth of partial melting appear to have remained constant throughout the ~210 000 year-long subaerial evolution of the Sete Cidades volcano. This is in contrast to most other oceanic volcanoes which are fed by magmas formed by variable degrees of partial melting or different depths (e.g. Woodhead, 1992). The relatively constant partial melting processes, and relatively constant melting depth, may be a result of adiabatic decompression induced melt generation at the ultraslow spreading axis of the Terceira rift, where the shape of the melting region remains the same as long as extensional movement continues. In contrast, the movement of a lithospheric plate across a mantle plume should lead to variable depths and degrees of partial melting, depending on the position of the volcano relative to the plume centre (Watson & McKenzie, 1991). The mantle source feeding the melting region beneath Sete Cidades differs significantly from that of the Agua de Pau volcano 20 km to the east (Fig. 11), implying that there is

a boundary dividing the ascending magmas and their sources (Haase & Beier, 2003). It is believed that melts in the mantle move by porous flow and an isotopic gradient would be expected between the two volcanoes if there was one large melting region in which magmas from different mantle source regions mixed during ascent. Consequently, the evidence for very limited mixing between the parental magmas of the two volcanoes suggests that two separate melting regions, with efficient focusing of magma into each volcano's plumbing system, exist beneath the Sete Cidades and Agua de Pau volcanoes.

Magma ascent and fractional crystallization processes of the Sete Cidades magmas

Geothermobarometry

The magmas of oceanic intraplate volcanoes frequently stagnate and differentiate at different crustal and even mantle levels during their ascent (Hansteen *et al.*, 1998b). Using the geothermobarometers of Putirka *et al.* (1996), Putirka (1999) and Putirka *et al.* (2003), the crystallization pressures and temperatures can be estimated from co-existing clinopyroxene phenocrysts and liquid compositions. Glass–clinopyroxene equilibrium calculations for primitive samples from Sete Cidades (SM0101 and SM0102: 5·5 and 6·5 wt % MgO, respectively) gave $1175 \pm 28\,^{\circ}C$ and $5·5 \pm 1·7$ kbar, representing a crystallization depth of $16·5 \pm 5$ km. Intermediate samples (SM160501–1) with 2·43 wt % MgO gave a slightly lower temperature of $1035\,^{\circ}C$ and pressures of $4·2 \pm 1·7$ kbar, which are within error of the more primitive lavas, although the data are somewhat displaced towards lower pressures. Renzulli & Santi (2000) estimated the temperatures and pressures of crystallization in the Sete Cidades basaltic magmas at $1222 \pm 62\,^{\circ}C$ and 4 kbar, respectively, whereas for the evolved rocks, they found $698 \pm 3\,^{\circ}C$ and 0·2–1·5 kbar using the ternary feldspar geothermometer of Fuhrman & Lindsley (1988) and the geobarometer of Green & Usdansky (1986). In our evolved samples from Sete Cidades, we did not find clinopyroxene–liquid equilibrium pairs using the standard error of estimate (SEE) method described by Putirka (1999). None of the Sete Cidades evolved lavas was, therefore, suitable for pressure estimates. However, Thurow & Hansteen (in preparation) determined a pressure of $1·1 \pm 0·3$ kbar ($3·5 \pm 1$ km) and a temperature of $817\,^{\circ}C$ from fluid inclusions in a co-magmatic hornblende gabbro xenolith interpreted as a solidified magma chamber wall fragment exhumed by the alkali basaltic Pico das Camarinhas eruption (Ponta da Ferraria; sample SM170501–32), resulting from short-term magma stagnation. They further found a lower crustal stagnation level at about $3·0 \pm 0·7$ kbar for the young alkali basaltic lavas from Mosteiros.

The geobarometric estimates for several basaltic lavas and pyroclastics suggest that the Sete Cidades primitive post-caldera magmas fractionated within the uppermost mantle close to the Moho, which is estimated to lie at about 14 km beneath the Azores platform (Luis *et al.*, 1998; Escartín *et al.*, 2001). Crystallization close to the crust–mantle boundary has also been observed in the Canary Islands and Hawaii (Putirka, 1997; Hansteen *et al.*, 1998b). The deep onset of crystallization requires a relatively cold and probably thick lithosphere above the melting region because the magmas are cooled to about 1150–1200 $^{\circ}C$ within the uppermost mantle. Such a relatively cold lithosphere within the Terceira spreading axis is consistent with geophysical models, showing that cooling is more efficient than heat transfer from the ascending mantle in ultraslow spreading regions (Reid & Jackson, 1981). Alternatively, the estimated fractionation depths within the uppermost mantle may correspond to the onset of degassing-induced crystallization, thus representing the depth of CO_2 oversaturation of the magmas. Such upper mantle crystallization has been proposed for Quaternary basanites on the Canary Islands, where CO_2 oversaturation and vigorous crystallization typically start at 40–25 km depth (Hansteen *et al.*, 1998a). After stagnation and crystallization at the crust–mantle boundary, the Sete Cidades magmas typically ascended rapidly to a shallow level of about 3·5 km depth. Such magmas evolved to trachytic compositions and fed the caldera-forming eruption. The occurrence of lower crustal xenoliths in young mafic flank eruptions at Sete Cidades strongly indicates that the magmas also resided intermittently within the lower crust. This is supported by fluid inclusion barometry of mafic and ultramafic xenoliths (Thurow & Hansteen, in preparation), and would imply that the young, mafic magmas could have chemically interacted with the island crust.

Upper mantle magma stagnation and fractional crystallization were also observed at La Palma (Klügel *et al.*, 2000; Klügel *et al.*, 2005), where the pressures were estimated at 4·1–7·7 kbar (average 6·0 kbar) using clinopyroxene–melt. Thus, the magmas were stored deeper in the lithosphere than beneath Sete Cidades, possibly as a result of the thicker, older and colder lithosphere beneath the Canary Islands, or as a result of the higher initial CO2 contents of the magmas. Additional crustal magma accumulation occurred within the lower crust at pressures of 2·4–4·7 kbar (average 3·3 kbar) beneath La Palma. Such multi-stage magma ascent and fractionation also occurs beneath other North Atlantic ocean islands (e.g. Madeira; Schwarz *et al.*, 2004).

Oxygen fugacity

Coexisting spinel and Fe–Ti oxides (preferentially cores) were used to determine the oxygen-fugacities of the
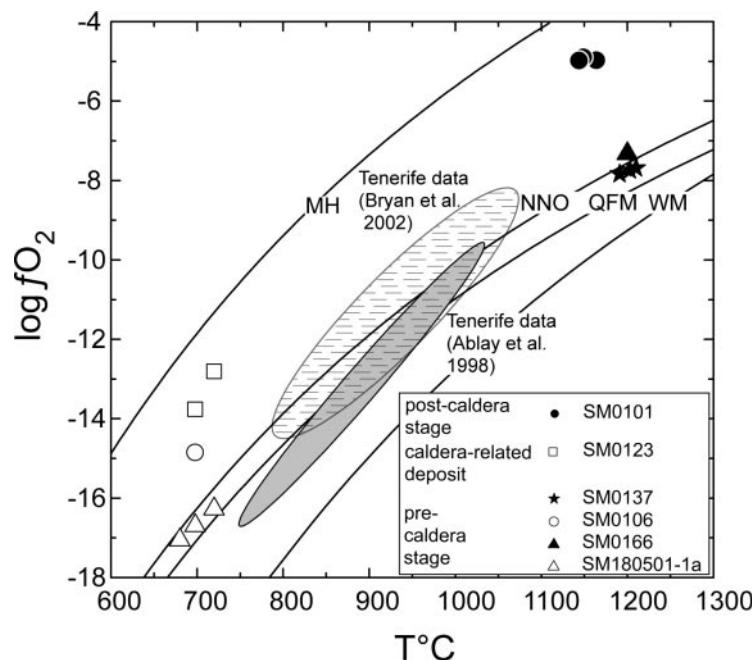
Fig. 13. Log fO_2 vs temperature (°C) for the Sete Cidades lavas compared with lavas from Tenerife (Ablay *et al.*, 1998; Bryan *et al.*, 2002). Filled symbols are basaltic samples; open symbols represent trachytic compositions.

magmas using the fugacity modelling program QUILF of Andersen *et al.* (1993). The equilibrium of the oxides was tested using the $\log(Mg/Mn)_{mag}$ and $\log(Mg/Mn)_{ilm}$ ratios of Bacon & Hirschmann (1988). The fO_2 of several lavas was determined and we find that a few basalts lie close to the Ni–NiO buffer curve similar to some evolved lavas from Tenerife (Fig. 13), although the Tenerife lavas formed in an open-system, hence they cross the oxygen buffer curves (Bryan *et al.*, 2002). On the other hand, one basalt and two trachyte samples show significantly higher fO_2. The pre-caldera samples have significantly lower fO_2 than the caldera-related deposits and post-caldera samples.

We propose that the higher fO_2 values probably reflect higher total volatile contents in the post-caldera magmas of Sete Cidades, in both the basaltic and trachytic compositions. This would also be an explanation for the more explosive style of the volcanism after the caldera-forming eruption. Therefore, the post-caldera mantle source must be characterized by a higher volatile component, increasing the $\log fO_2$ in the younger lavas. One possibility to increase the volatile content of a magma would be the assimilation of crustal rocks, consistent with the occurrence of crustal xenoliths in the lavas of Ponta da Ferraria and Mafra.

Fractional crystallization and modelling using MELTS

Based on the petrological observations and the geochemical data, the following phases crystallized from the Sete Cidades magmas: olivine, clinopyroxene, magnetite, ilmenite, plagioclase, apatite, alkali feldspar, amphibole and biotite. The major element composition of the Sete Cidades lavas indicates that the samples lie along a single liquid line of descent (Fig. 8), although the slight differences in incompatible trace element (e.g. Ba/Nb, La/Nb) and radiogenic isotope ratios (Figs 10 and 11) imply that the magmas are not all comagmatic. The fractionation of olivine leads to decreasing MgO and Ni contents (Fig. 9), whereas the decrease of CaO (Fig. 8) can be explained by the crystallization of clinopyroxene from magmas with MgO contents of between 12 and 3 wt %, and plagioclase at MgO contents of <3 wt %. Plagioclase also occurs in the more primitive rocks, but is modally of minor importance; the enrichment in Al_2O_3 in lavas with between 16 and 2 wt % MgO also suggests minor fractionation of plagioclase. The sharp decrease in Al_2O_3 content at ~2 wt % MgO shows that crystallization of feldspars dominates the fractionation assemblage in the evolved rocks (Fig. 8). The crystallization of ilmenite and magnetite decreases the concentrations of TiO_2 and FeO^T in the lavas with less than 6 wt % MgO. The decreasing P_2O_5 content at MgO contents below 3 wt % as a result of the fractionation of apatite.

The major element compositions of the Sete Cidades rocks can be fitted by a fractional crystallization trend calculated using MELTS (Ghiorso, 1997) with sample SM0140 as the parent magma (Fig. 8). The oxygen fugacity has been estimated at $\log fO_2 = -10$ using co-existing Fe–Ti oxides (Fig. 13). At a pressure

of 5 kbar and estimated H_2O and CO_2 contents of 0·5 wt %, MELTS calculates a liquidus temperature of 1311 °C for sample SM0140. The actual trends from Sete Cidades and the modelled MELTS fractionation trends fit relatively well, confirming that the major element compositional variation of the Sete Cidades lavas is mainly a result of fractional crystallization processes. Contrary to other oceanic intraplate volcanoes (e.g. Tenerife; Ablay *et al.*, 1998; Bryan *et al.*, 2002), Sete Cidades does not show a bimodal distribution of the lava compositions. The occurrence of bimodal lava compositions in many magmatic systems has been explained in terms of a density barrier for intermediate magmas, i.e. as a result of the increased Fe contents of intermediate magmas which are too dense to rise to the surface in most regions (Stolper *et al.*, 1981). The Fe content does not increase significantly during crystal fractionation in the Sete Cidades magmas (Fig. 8) and this could explain the eruption of the entire compositional range of magmas. The fractional crystallization model using the MELTS program supports this conclusion because the melt density is predicted to decrease continuously from the primitive magma starting composition of SM0140 (2·77 g/cm^3) to 2·52 g/cm^3 in the trachytic melts.

Effects of fractional crystallization processes on incompatible element ratios

The coherent fractional crystallization trend allows us to determine the effects of fractionation of different mineral phases on the abundances of incompatible elements and their ratios. Understanding the effects of crystal fractionation processes on incompatible element concentrations and ratios is important because highly incompatible element ratios in lavas are often used as a proxy for the compositions of the mantle source of the lavas (e.g. Kamber & Collerson, 2000*a*). The Nb/Zr ratio is not affected by crystal fractionation processes (Fig. 10a), implying that these two elements have similar distribution coefficients and can be used to distinguish different mantle sources (Kamber & Collerson, 2000*b*). In contrast, the highly incompatible element ratios Nb/Ta and Zr/Hf both increase significantly with decreasing MgO in the Sete Cidades sample suite (Fig. 10b and d), showing that Nb and Zr are more incompatible than Ta and Hf, respectively, during fractional crystallization. Consequently, the use of these element ratios to compare the mantle sources of different suites of rocks is limited by the effects of fractional crystallization processes. The increasing Zr/Hf in OIB has been explained by the fractionation of clinopyroxene (David *et al.*, 2000). However, whereas the increasing (La/Sm)$_N$ ratios in the more evolved lavas can be explained by extensive fractionation of clinopyroxene (Fig. 14a), a model using recently published clinopyroxene distribution coefficients

(Hart & Dunn, 1993) and 55% clinopyroxene in the fractionating mineral assemblage fails to reproduce the observed Zr/Hf trend (Fig. 14b). Increasing Nb/Ta in alkaline lava series has been attributed to the presence of titanite in the fractionating assemblage (Wolff, 1984; Green, 1995); however, the Sete Cidades alkali basalts do not contain titanite. Other phases such as olivine and plagioclase that crystallize from the Sete Cidades alkali basalts have only low contents of Zr, Hf, Nb and Ta, and do not show large differences between the distribution coefficients of the respective elements (Green, 1995). Thus, the partition coefficients of Nb relative to Ta, and Zr relative to Hf for the Sete Cidades clinopyroxenes may be too low, especially because they are Ti augites. Alternatively, extensive magnetite fractionation could explain the trends; Green & Pearson (1987) have shown that Nb ($K_D = 0.40$) and Zr ($K_D = 0.10$) are more incompatible than Ta ($K_D = 1.0–10$) and Hf ($K_D = 2.0–4.0$), respectively, in magnetite.

The trace elements Ba, Eu and Sr are depleted in the evolved rocks, supporting the late-stage fractionation of feldspar. The decreasing La/Nb at about 3 wt % MgO coincides with the onset of apatite fractionation (Fig. 8f) and, probably, apatite depletes the magma in La relative to Nb (Fujimaki, 1986). Only the most evolved lavas show low Ba/Nb, possibly as a result of the late-stage fractionation of biotite, withdrawing preferentially Ba ($K_D^{Biotite/Melt} \sim 23.5$) relative to Nb ($K_D^{Biotite/Melt} \sim 6.4$) (Nash & Crecraft, 1985). We conclude that in alkaline rock series, even the ratios of highly incompatible elements can be fractionated; this has to be considered when these ratios are used to constrain the compositions of the mantle sources of lavas from different volcanoes.

Time-scales of magma evolution and ascent beneath Sete Cidades

The stratigraphy at Sete Cidades show several fractionation cycles from basaltic to trachytic compositions over the last 210 000 years (Moore, 1991*b*). The Sete Cidades post-caldera stage consists of 11 changes between basaltic and trachytic compositions in the last 16 000 years. The trachytic post-caldera eruptions were mostly erupted from the caldera vent, suggesting the existence of a shallow magma chamber beneath the centre of the volcano, whereas all the post-caldera basalts were erupted from flank vents along rift zones, thereby generating the alternating post-caldera stage stratigraphy. Consequently, there appears to be no connection between the trachytic magma chamber and the basaltic magma systems on the volcano flanks. In contrast, the subaerial pre-caldera stage observed in the Sete Cidades caldera wall contains at least seven compositional changes from 210 000 to 36 000 years (Fig. 3), and these lavas erupted from the central summit only. On average, the composition
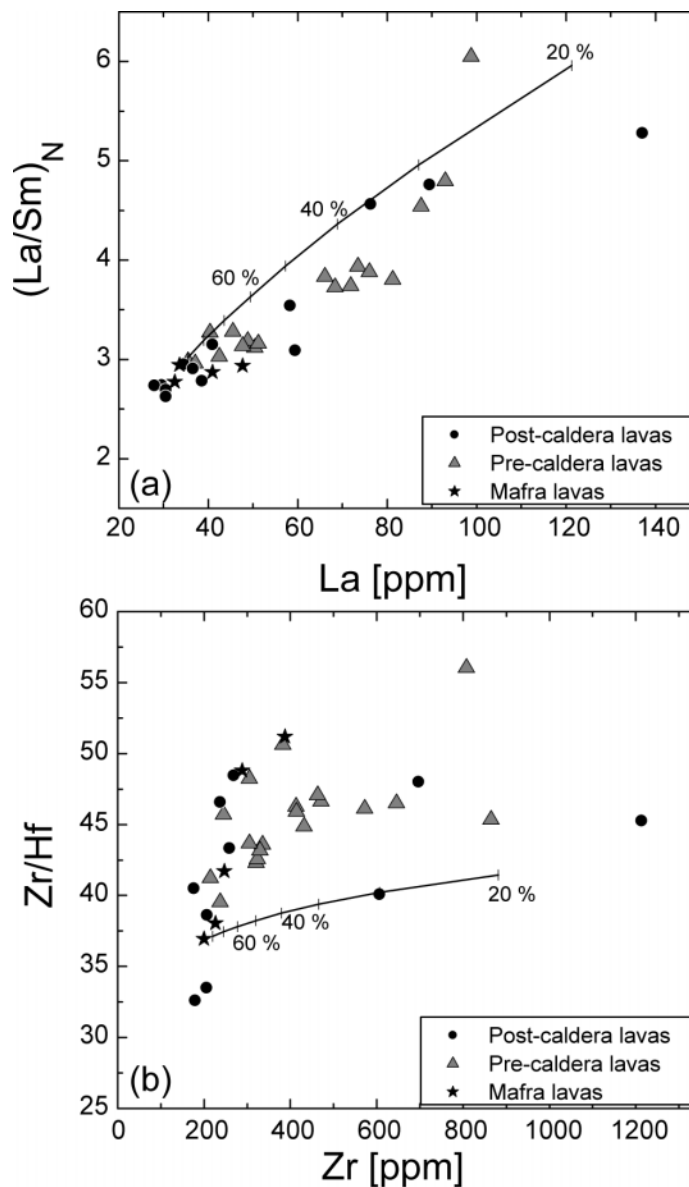
Fig. 14. Fractionation trends for (a) (La/Sm)$_N$ vs La and (b) Zr/Hf vs Zr for 10% increments of a crystallization assemblage with 55% clinopyroxene, 35% olivine, 5% plagioclase, 4% ilmenite and 1% apatite. Tick marks represent degrees of Raleigh fractionation in increments of 10%. Partition coefficients for La, Zr and Hf in olivine are from Zanetti *et al.* (2004); Sm in olivine and plagioclase from Dunn and Sen (1994); clinopyroxene from Hart and Dunn (1993); magnetite from Nielsen *et al.* (1992); apatite from Fujimaki (1986).

changed every 25 000 years in the pre-caldera stage, consistent with observations on the neighbouring Agua de Pau volcano (Widom *et al.*, 1992, 1993). Similar temporal compositional variations have been found on Tenerife, where two different time-scales have to be taken into consideration. First, the overall differentiation time from a basanitic to a phonolitic composition, including the formation of a shallow magma chamber, is ~200 000 years (Hawkesworth *et al.*, 2000). Secondly, fractionation within trachytic magmas occurs within shorter time-scales of 100 to 1000 s of years. These

short-term fractionation scales have not been observed at Sete Cidades, but the overall differentiation from a dominantly basaltic to a dominantly trachytic eruptive stage seems to be of the same temporal order at both volcanoes.

The trachytic caldera-forming eruption was probably triggered by basaltic replenishment of the shallow magma chamber, indicated by the occurrence of olivine xenocrysts (Fo$_{81}$) and inversely zoned clinopyroxene xenocrysts. The large compositional variation of the streaky glass shards in the caldera-forming deposits

suggests mixing between an evolved magma and a basaltic magma in equilibrium with olivine with Fo_{81} (Fig. 12). Such a basaltic replenishment into an evolved magma chamber could also explain the occurrence of opacitized rims around kaersutite crystals (SM0137), as the heating of an evolved to intermediate magma by the intrusion of hot basaltic magma may raise the magma temperature into the Ca–pyroxene stability field (855 °C, 0·13 GPa; Rutherford & Devine, 2003). The intrusion of a hot basaltic magma into an evolved magma could also result in reversely zoned clinopyroxene and plagioclase crystals. However, although a few clinopyroxene xenocrysts are reversely zoned, with increasing Mg-number towards the rim, the majority of the clinopyroxene crystals show normal zoning, making decompression more likely, where the formation of new mineral phases can be used as an indicator of magma ascent rate (Rutherford & Devine, 1988; Rutherford & Hill, 1993). These authors concluded that Fe oxide dehydration rims on amphibole form either by decreasing H_2O in the melt during magma ascent or during magma chamber storage. Decreasing H_2O in the Sete Cidades magmas seems unlikely, as this would not result in the decompression textures observed in the plagioclase xenocrysts. The experiments show that amphiboles without reaction rims ascended from 8 km depth to the surface in less than 5 days, and that the thickness of the rims correlates with the storage time at less than 6·5 km depth (Rutherford & Devine, 1988; Nicholis & Rutherford, 2004). The kaersutite reaction rims in sample SM0137 show minimum widths of 100 μm and a maximum width of 200 μm, measured from back-scattered electron images. The experiments of Rutherford and Hill (1993) gave a rim width of 30–50 μm for an experimental stagnation time of 9–17 days. We conclude that some of the Sete Cidades magmas (e.g. sample SM0137) resided at maximum for a few weeks in a shallow magma chamber at ∼3·5 km depth until they ascended to the surface.

Temporal variations in the petrogenesis of the Sete Cidades lavas

The fact that there is no systematic change in the major and in most trace element compositions of the primitive magmas of the pre- and post-caldera lavas at Sete Cidades indicates that mantle partial melting processes did not change significantly during the last 210 000 years. In this respect, the magmatic evolution of the Sete Cidades volcano differs from the systematic temporal variation in the degree of partial melting observed at most oceanic intraplate volcanoes (e.g. Woodhead, 1992). However, the variation of $(La/Sm)_N$, Ba/Nb and La/Nb ratios, as well as of Sr and Nd isotope compositions, suggests small-scale heterogeneity within the Sete Cidades mantle source and binary mixing, with the two end-member components having varying influences with time (Figs 10 and 11). Thus, the post-caldera lavas have higher Ba/Nb, but lower $(La/Sm)_N$ and Nb/La, than the pre-caldera lavas, indicating a slight systematic change in the mantle source at the time of caldera formation. Because the post-caldera magmas have higher Ba/Nb (Fig. 10c), and Ba is more incompatible than Nb, this variation cannot be a result of increasing depletion of the source because of the previous melting events forming the pre-caldera magmas, as observed at other volcanoes (e.g. Reiners, 1998). On a smaller scale, the stratigraphic section at Ponta da Ferraria (Fig. 3) shows slight variations in the pre-caldera magma sources with time (Fig. 15). For example, the lower lavas in the Ponta da Ferraria section have higher $^{87}Sr/^{86}Sr$ and Ba/Nb than the upper lavas (Fig. 15). These variations reflect changes in the mantle source of the pre-caldera magmas rather than increasing depletion of the source because other incompatible element ratios such as Nb/Zr or $(La/Sm)_N$ do not decrease towards the upper part of the section.

One notable systematic difference between the pre- and post-caldera lavas is the MgO content of the two lava series; the pre-caldera lavas exhibit a continuous compositional range of between 11 and 0 wt % MgO (Fig. 8). In contrast, the post-caldera stage is divided into trachytic eruptions in the caldera, and basaltic eruptions with more than 6 wt % MgO on the flank, i.e. the post-caldera stage shows an apparently bimodal distribution. This change in the magma evolution may be a result of the presence of a shallow magma chamber that developed at the end of the pre-caldera stage of the Sete Cidades volcano and may have acted as a density barrier, preventing the eruption of primitive lavas from the caldera vent during the post-caldera stage. As long as the felsic magma chamber existed, the basaltic and intermediate lavas were erupted along the volcano's flanks, e.g. at Mafra and Ponta da Ferraria (Figs 1, 2 and 3). The post-caldera stage is dominated by very primitive basaltic flank eruptions (Ponta da Ferraria, Mafra) and a few coeval trachytic eruptions within the caldera. For example, the trachytic eruption of Caldera Seca (Inner Caldera) occurred ∼500 years ago, whereas the alkali basalts of Ponta da Ferraria (western flank) erupted 840 years ago (Moore, 1990). The youngest flank eruptions, including Mafra and Ponta da Ferraria, contain abundant mafic and ultramafic xenoliths, implying relatively short crustal residence times. High magma supply rates into the lithosphere during the pre-caldera stage may have induced the formation of a stable magma reservoir in which relatively evolved magmas formed by crystal–liquid fractionation. A decreased magma production rate since caldera formation has resulted in only small-volume eruptions of relatively primitive magmas on the flanks of Sete Cidades.
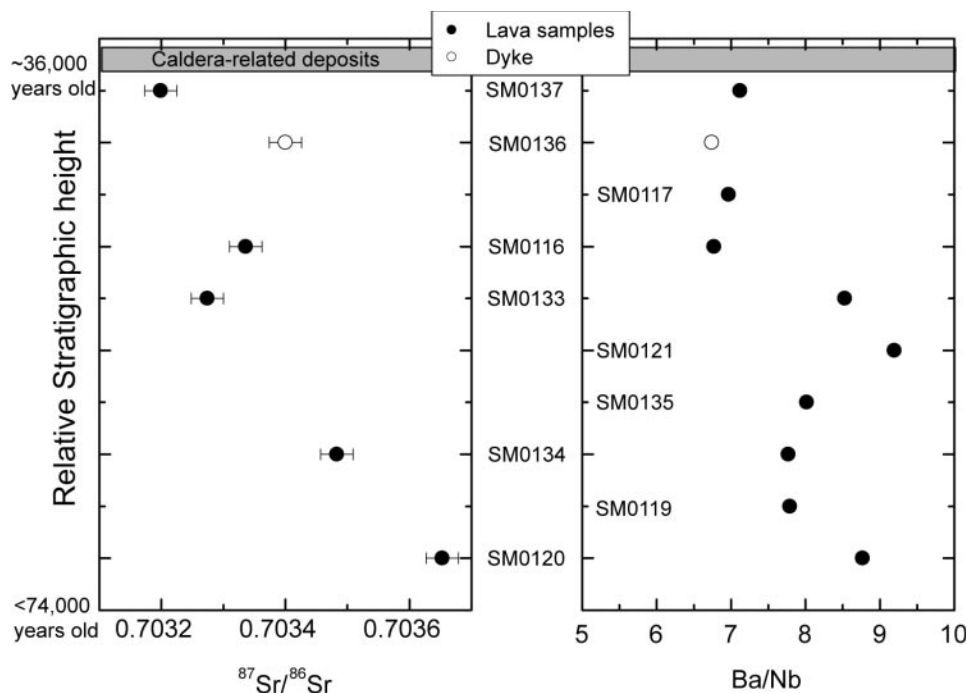
Fig. 15. Variation of the pre-caldera $^{87}Sr/^{86}Sr$ and Ba/Nb ratios with stratigraphic height in the sea-cliff section at Ponta da Ferraria. The stratigraphic heights represent an age range from <74 000 to ~36 000 years (Moore & Rubin, 1991; Pacheco *et al.*, 2005). The lower lava flows have a distinct composition from the upper units. The error bar represents a maximum 2σ-error of 0·00026.

In summary, three important differences exist between the pre- and post-caldera rocks: (1) a higher oxygen fugacity in the post-caldera basalts; (2) differences in some incompatible trace element ratios in the primitive post-caldera samples (e.g. higher Ba/Nb, La/Nb, lower La/Sm$_N$), and (3) a bimodal distribution in the post-caldera lavas, contrasting with a continuous lava trend in the pre-caldera stage.

Evidence for magma mixing?

The Sete Cidades alkali basalts frequently contain olivine xenocrysts with large compositional variations and Fo contents between 52 and 90. The intermediate and evolved lavas contain reversely zoned clinopyroxene xenocrysts (e.g. SM0137, SM0149), suggesting crystallization from different magmas and thus, probably, magma mixing processes. The plagioclase crystals in the intermediate lavas also show a large compositional range; the presence of anorthite-rich crystals which accumulated from a more primitive magma is consistent with the occurrence of reversely zoned clinopyroxenes. In one of these samples (SM0108), a sanidine phenocryst was also observed, suggesting that the primitive and intermediate magmas assimilated crystals of more evolved magmas before the eruption. Consequently, the replenishment of the evolved magma chamber by basaltic liquids appears

to have occurred frequently during the evolution of the volcano and may have been the trigger for eruptions.

The initiation of the caldera-forming eruption of the Sete Cidades volcano about 16 000–36 000 years ago also appears to be related to magma mixing. Calderas are formed by extensive, explosive eruptions emptying the magma chamber, during which the roof sags into the magma chamber and may leave pockets of remaining melt that can erupt through the caldera-ring faults and form eruption centres on the inner caldera ring (Folch *et al.*, 2001). Two mechanisms may be responsible for the initiation of the caldera-forming eruptions: (1) step-wise degassing of intermediate and trachytic magma may lead to the sagging of the magma chamber roof (Gudmundsson, 1998); or (2) hot basaltic magma injections into a magma chamber containing a cooler, evolved magma, leading to vigorous convection and a pressure increase in the magma chamber triggering an explosive eruption (Sparks *et al.*, 1977). The glasses of the caldera outflow deposit contain elongated glassy shards with very heterogeneous compositions (Fig. 12). The glass chemical data of the outflow pyroclastic deposit mostly lie on linear trends that probably reflect mixing between a trachytic and a more primitive melt. The trachytic glass SM0123 from the caldera outflow deposit has Mg-numbers of 19–33, but contains rare olivines with Fo$_{81}$ which would be in equilibrium with a liquid of Mg-number of ~50, supporting mixing of a trachytic melt with a basalt with

MgO of about 5 wt %. Further evidence is given by the occurrence of inversely zoned clinopyroxene xenocrysts with a higher Mg-number in the crystal's rim than in its core. Consequently, a possible explanation is the intrusion of a hot, more primitive basaltic melt into a cooler evolved melt stored in a crustal reservoir, leading to overheating of the trachytic magma (Sparks *et al.*, 1977). We conclude that the caldera-related eruptions have been triggered by the inflow of hot basaltic melt into a shallow magma chamber containing trachytic magma.

Nine alkali basaltic samples from the Mafra flank eruption (Figs 1 and 2) were analysed and show variations of 1·08–1·40 wt % K_2O, Nb/Zr of 0·19–0·23, $^{143}Nd/^{144}Nd$ of 0·51291–0·51280 and $^{87}Sr/^{86}Sr$ of 0·70361–0·70414, suggesting compositionally distinct magma sources feeding this single eruption. The lava (SM0102; Table 1) with the highest $^{87}Sr/^{86}Sr$ comes from the lava delta most distant from the eruptive fissure, whereas sample SM0101 of intermediate composition is slightly closer, and the relatively unradiogenic sample SM0161 was taken from the youngest cinder cone on this fissure, possibly indicating a temporal decrease in the Sr isotope ratios. Thus, the Mafra eruption apparently shows chemical evolution of its products similar to the variations observed, e.g. during the Puu Oo eruption of Kilauea volcano, Hawaii (Garcia *et al.*, 1996). The temporal compositional variation in oceanic basalts has been explained by crustal contamination, different degrees of partial melting, or mixing of melts from chemically distinct sources (e.g. Reiners, 2002). Crustal contamination within the oceanic crust leading to lower $^{143}Nd/^{144}Nd$ appears unlikely beneath Sete Cidades volcano because both the MORB-like oceanic crust and the lavas of the volcano have higher Nd isotope ratios than the Mafra lavas. The constant major element compositions (e.g. Na_2O, FeO^T) and trace element ratios (e.g. Ce/Yb, Sm/Yb) of the Mafra lavas imply similar degrees of partial melting of the magmas feeding the eruption. Thus, the Mafra basalts appear to show the increased influence of another mantle source which resembles that of the neighbouring volcano, Agua de Pau, which has much higher Sr isotope but lower Nd isotope ratios (Fig. 11a). Probably, the trend of the Mafra lavas indicates mixing between a magma of typical Sete Cidades composition and a magma derived from the Agua de Pau mantle source. Such a mixing process is supported by the broad linear positive correlation between $^{87}Sr/^{86}Sr$ and Rb/Sr (Fig. 11b), ranging between the compositions of Sete Cidades and Agua de Pau lavas. Thus, we speculate that a small volume of magma from the Agua de Pau source must have been present beneath the western flank of the Sete Cidades volcano giving rise to the unusually radiogenic lavas. This is surprising given the relative homogeneity of the rest of the studied lavas from Sete Cidades. Interestingly, the different Mafra lavas also plot on mixing lines between whole-rock–glass compositions and olivine (Fig. 9), suggesting that the magmas also entrained large volumes of xenocrystic olivine during their ascent.

CONCLUSIONS

The geochemical and petrological results of this study, combined with stratigraphic observations, show that over the last 210 000 years, the lavas of the Sete Cidades volcano have undergone frequent changes between primitive and evolved compositions. These alternations occurred during the main shield-building stage that contains intercalated trachytic deposits (>210 000–36 000 years) which form the greater part of the subaerial volume. A series of caldera-forming eruptions occurred from 36 000 to 16 000 years ago, producing mainly trachytic pyroclastic deposits. The post-caldera stage and recent volcanism have been dominated by both trachytic eruptions within the caldera and along the caldera ring fault and coeval basaltic eruptions from parasitic craters around the flanks of the volcano (Fig. 16). Major element and most trace element compositions of all lavas of Sete Cidades volcano show that the magmas evolved mainly by crystal fractionation processes, whilst partial melting processes and mantle sources remained relatively constant throughout the evolution of the subaerial part of the volcano, i.e. over a period of time of 210 000 years. However, a slight systematic difference in the Ba/Nb, La/Nb and the Sr isotope ratios between the pre- and post-caldera lavas implies that the caldera eruption event coincided with a change in magma source compositions. Thermobarometric calculations indicate that the basaltic magmas started to fractionate close to the crust–mantle boundary, at about 16 ± 5 km depth, implying that the ultraslow Terceira rift spreading axis is overlain by a relatively cold lithosphere. The more evolved magmas fractionated extensively in a shallow magma chamber at about 3·5 km depth beneath the volcano, whereas basaltic magmas resided for only short periods of time in crustal reservoirs (Fig. 16). After caldera formation, residual trachytic magma erupted as lava within the caldera. The more primitive post-caldera magmas reflect rejuvenation of the magmatic system of Sete Cidades volcano and continuing activity along the volcano's rift zone in the Terceira rift. These lavas have the most primitive compositions and contain abundant olivine and clinopyroxene phenocrysts as well as mantle xenoliths, suggesting a relatively fast magma ascent. The alkali volcanic series of Sete Cidades shows clear evidence for fractional crystallization processes in both the major element whole-rock chemistry and in the trace element compositions. The variations observed in the radiogenic isotopes and in the trace element ratios suggest that the lavas from Sete
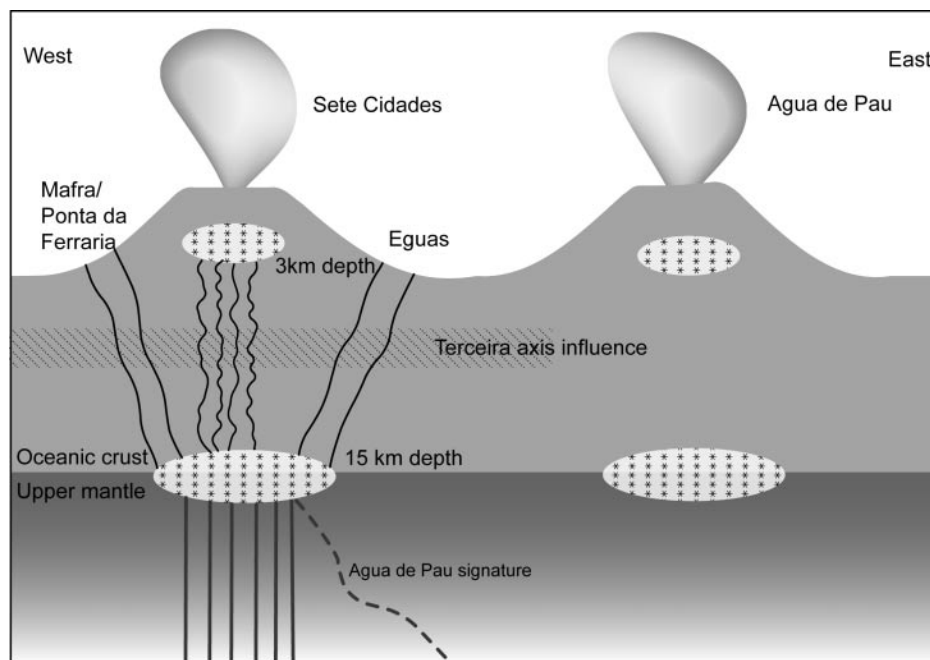
Fig. 16. Schematic sketch of the Sete Cidades volcano comprising two storage levels (3 and 15 km). The magmas forming the post-caldera flank eruptions bypassed the shallow magma chamber. Mixing between the Sete Cidades volcanic systems and the Agua de Pau magmas probably occurs in the upper mantle rather than in the oceanic crust.

Cidades formed from a mantle source which was heterogeneous on a small scale. The mantle source of the Sete Cidades basalts has a distinct composition compared with that of the adjacent Agua de Pau volcano, situated some 20 km further to the east. Only very limited interaction appears to take place between the two neighbouring magmatic systems; however, one of the most recent eruptions on the western flanks of Sete Cidades was fed partly by magmas from the Agua de Pau source.

ACKNOWLEDGMENTS

REFERENCES

Abdel Monem, A. A., Fernandez, L. A. & Boone, G. M. (1975) K–Ar ages from the eastern Azores group (Santa Maria, Sao Miguel and the Formigas islands). *Lithos* **8**, 247–254.

Ablay, G. J., Carroll, M. R., Palmer, M. R., Martí, J. & Sparks, R. S. J. (1998) Basanite–phonolite lineages of the Teide–Pico Viejo Volcanic Complex Tenerife, Canary Islands. *Journal of Petrology* **39**, 905–936.

Abouchami, W., Galer, S. J. G. & Hofmann, A. W. (2000) High precision lead isotope systematics of lavas from the Hawaiian Scientific Drilling Project. *Chemical Geology* **169**, 187–209.

Andersen, D. J., Lindsley, D. H. & Davidson, P. M. (1993) QUILF: a Pascal program to assess equilibria among Fe–Mg–Mn–Ti oxides, pyroxenes, olivine, and quartz. *Computers and Geosciences* **19**, 1333–1350.

Bacon, C. R. & Hirschmann, M. M. (1988) Mg/Mn partitioning as a test for equilibrium between coexisting Fe–Ti oxides. *American Mineralogist* **73**, 57–61.

Booth, B., Croasdale, R. & Walker, G. P. L. (1978) A quantitative study of five thousand years of volcanism on Sao Miguel, Azores. *Philosophical Transactions of the Royal Society of London* **288**, 271–319.

Bryan, S. E., Marti, J. & Leosson, M. (2002) Petrology and geochemistry of the Bandas del Sur Formation, Las Canadas Edifice, Tenerife (Canary Islands). *Journal of Petrology* **43**, 1815–1856.

Burnham, C. W. (1979) The importance of volatile constituents. In: Yoder, H. S., Jr (ed.) *The Evolution of the Igneous Rocks: Fiftieth Anniversary Perspectives.* Princeton, NJ: Princeton University Press, pp. 439–482.

Chen, C.-Y. & Frey, F. A. (1983) Origin of Hawaiian tholeiite and alkalic basalt. *Nature* **302**, 785–789.

Clague, D. A. (1987) Hawaiian alkaline volcanism. In: Fitton, J. G. & Upton, B. G. J. (eds) *Alkaline Igneous Rocks. Geological Society Special Publications*, 227–252.

David, K., Schiano, P. & Allegre, C. J. (2000) Assessment of the Zr/Hf fractionation in oceanic basalts and continental materials during petrogenetic processes. *Earth and Planetary Science Letters* **178**, 285–301.

Davies, G. R., Norry, M. J., Gerlach, D. C. & Cliff, R. A. (1989) A combined chemical and Pb–Sr–Nd isotope study of the Azores and Cap Verde hot-spots: the geodynamic implications.

In: Saunders, A. D. & Norry, M. J. (eds) *Magmatism in the Oceanic Basins. Geological Society Special Publications*, 231–255.

Droop, G. T. R. (1987) A general equation for estimating Fe (super 3+) concentrations in ferromagnesian silicates and oxides from microprobe analyses, using stoichiometric criteria. *Mineralogical Magazine* **51**, 431–435.

Dunn, T. & Sen, C. (1994) Mineral/matrix partition coefficients for orthopyroxene, plagioclase, and olivine in basaltic to andesitic systems; a combined analytical and experimental study. *Geochimica et Cosmochimica Acta* **58**, 717–733.

Escartín, J., Cannat, M., Pouliquen, G. & Rabain, A. (2001) Crustal thickness of V-shaped ridges south of the Azores: interaction of the Mid-Atlantic Ridge (36°–39°N) and the Azores hot spot. *Journal of Geophysical Research* **106**, 21, 719–721, 735.

Ewart, A. (1981) The mineralogy and chemistry of the anorogenic Tertiary silicic volcanics of S.E. Queensland and N.E. New South Wales, Australia. In: *Granites and Rhyolites*. Washington, DC: American Geophysical Union, pp. 10242–10256.

Feraud, G., Kaneoka, I. & Allègre, C. J. (1980) K/Ar ages and stress pattern in the Azores: geodynamic implications. *Earth and Planetary Science Letters* **46**, 275–286.

Folch, A., Codina, R. & Marti, J. (2001) Numerical modeling of magma withdrawal during explosive caldera-forming eruptions. *Journal of Geophysical Research* **106**, 16163–16175.

Frey, F. A. & Rhodes, J. M. (1993) Intershield geochemical differences among Hawaiian volcanoes: implications for source compositions, melting processes and magma ascent paths. *Philosophical Transactions of the Royal Society of London* **A342**, 121–136.

Frey, F. A., Garcia, M. O. & Roden, M. F. (1994) Geochemical characteristics of Koolau Volcano: implications of intershield geochemical differences among Hawaiian volcanoes. *Geochimica et Cosmochimica Acta* **58**, 1441–1462.

Fuhrman, M. L. & Lindsley, D. H. (1988) Ternary–feldspar modeling and thermometry. *American Mineralogist* **73**, 201–215.

Fujimaki, H. (1986) Partition coefficients of Hf, Zr, and REE between zircon, apatite, and liquid. *Contributions to Mineralogy and Petrology* **94**, 42–45.

Garbe-Schönberg, C.-D. (1993) Simultaneous determination of thirty-seven trace elements in twenty-eight international rock standards by ICP-MS. *Geostandards Newsletters* **17**, 81–97.

Garcia, M. O., Rhodes, J. M., Trusdell, F. A. & Pietruszka, A. J. (1996) Petrology of lavas from the Puu Oo eruption of Kilauea Volcano: III. The Kupaianaha episode (1986–1992). *Bulletin of Volcanology* **58**, 359–379.

Geldmacher, J., van den Bogaard, P., Hoernle, K. & Schmincke, H. U. (2000) The ^{40}Ar/^{39}Ar age dating of the Madeira Archipelago and hotspot track (eastern North Atlantic). *Geochemistry, Geophysics, Geosystems* **1**.

Ghiorso, M. S. (1997) Thermodynamic models of igneous processes. *Annual Reviews of Earth and Planetary Sciences* **25**, 221–241.

Ghiorso, M. S. & Sack, R. O. (1993) MELTS; software for the thermodynamic analysis of phase equilibria in magmatic systems. In: *Geological Society of America, 1993 Annual Meeting*. Boulder, CO: Geological Society of America (GSA), p. 96.

Govindaraju, K. (1995) Working values with confidence limits of twenty-six CRPG, ANRT and IWG–GIT Geostandards. *Geostandards Newsletter* **19**, 1–32.

Green, N. L. & Usdansky, S. I. (1986) Ternary–feldspar mixing relations and thermobarometry. *American Mineralogist* **71**, 1100–1108.

Green, T. H. (1995) Significance of Nb/Ta as an indicator of geochemical processes in the crust–mantle system. *Chemical Geology* **120**, 347–359.

Green, T. H. & Pearson, N. J. (1987) An experimental study of Nb and Ta partitioning between Ti-rich minerals and silicate liquids at high pressure and temperature. *Geochimica et Cosmochimica Acta* **51**, 53–62.

Griffiths, R. W. & Richards, M. A. (1989) The adjustment of mantle plumes to changes in plate motion. *Geophysical Research Letters* **16**, 437–440.

Gudmundsson, A. (1998) Formation and development of normal-fault calderas and the initiation of large explosive eruptions. *Bulletin of Vulcanology* **60**, 160–170.

Haase, K. M. & Beier, C. (2003) Tectonic control of ocean island basalt sources on Sao Miguel, Azores? *Geophysical Research Letters* **30**, 1856.

Hansteen, T. H. & Troll, V. R. (2003) Oxygen isotope composition of xenoliths from the oceanic crust and volcanic edifice beneath Gran Canaria (Canary Islands): consequences for crustal contamination of ascending magmas. *Chemical Geology* **193**, 181–193.

Hansteen, T. H., Gurenko, A. A., Weaver, P. P. E., Schmincke, H.-U., Firth, J., Baraza, J. F., *et al.* (1998*a*) Sulfur, chlorine, and fluorine in glass inclusions in olivine and clinopyroxene from basaltic hyaloclastites representing the Gran Canaria shield stage at Sites 953 and 956. *Proceedings of the Ocean Drilling Program, Scientific Results* **157**, 403–410.

Hansteen, T. H., Kluegel, A. & Schmincke, H.-U. (1998*b*) Multi-stage magma ascent beneath the Canary Islands; evidence from fluid inclusions. *Contributions to Mineralogy and Petrology* **132**, 48–64.

Hart, S. R. & Davis, K. E. (1978) Nickel partitioning between olivine and silicate melt. *Earth and Planetary Science Letters* **40**, 203–219.

Hart, S. R. & Dunn, T. (1993) Experimental cpx/melt partitioning of 24 trace elements. *Contributions to Mineralogy and Petrology* **113**, 1–8.

Hawkesworth, C. J., Norry, M. J., Roddick, J. C. & Vollmer, R. (1979) ^{143}Nd/^{144}Nd and ^{87}Sr/^{86}Sr ratios from the Azores and their significance in LIL-element enriched mantle. *Nature* **280**, 28–31.

Hawkesworth, C. J., Blake, S., Evans, P., Hughes, R., MacDonald, R., Thomas, L. E., *et al.* (2000) Time scales of crystal fractionation in magma chambers: integrating physical, isotopic and geochemical perspectives. *Journal of Petrology* **41**, 991–1006.

Hess, P. C. (1992) Phase equilibria constraints on the origin of ocean floor basalts. In: Phipps Morgan, J., Blackman, D. K. & Sinton, J. M. (eds) *Mantle Flow and Melt Generation at Mid-Ocean Ridges. American Geophysical Union*, 67–102.

Hoernle, K. & Schmincke, H. U. (1993) The role of partial melting in the 15-Ma geochemical evolution of Gran Canaria: a blob model for the Canary hotspot. *Journal of Petrology* **34**, 599–626.

Hoernle, K., Tilton, G. & Schmincke, H.-U. (1991) Sr–Nd–Pb isotopic evolution of Gran Canaria: evidence for shallow enriched mantle beneath the Canary Islands. *Earth and Planetary Science Letters* **106**, 44–63.

Johnson, C. L., Wijbrans, J. R., Constable, C. G., Gee, J., Staudigel, H., Tauxe, L., *et al.* (1998) ^{40}Ar/^{39}Ar ages and paleomagnetism of Sao Miguel lavas, Azores. *Earth and Planetary Science Letters* **1160**, 637–649.

Kamber, B. S. & Collerson, K. D. (2000*a*) Role of 'hidden' deeply subducted slabs in mantle depletion. *Chemical Geology* **166**, 241–254.

Kamber, B. S. & Collerson, K. D. (2000*b*) Zr/Nb systematics of ocean island basalts reassessed: the case for binary mixing. In: *In commemoration of Keith Gordon Cox, 1933–1998*. Oxford: Oxford University Press, 1007–1021.

Klügel, A., Hoernle, K. A., Schmincke, H.-U. & White, J. D. L. (2000) The chemically zoned 1949 eruption on La Palma (Canary Islands): petrologic evolution and magma supply dynamics of a rift zone eruption. *Journal of Geophysical Research* **105**, 5997–6016.

Klügel, A., Hansteen, T. H. & Galipp, K. (2005) Magma storage and underplating beneath Cumbre Vieja volcano, La Palma (Canary Islands). *Earth and Planetary Science Letters* **236**, 211–226.

Krause, D. C. & Watkins, N. D. (1970) North Atlantic crustal genesis in the vicinity of the Azores. *Geophysical Journal of the Royal Astronomical Society* **19**, 261–283.

Le Maitre, R. W., Bateman, P., Dudek, A., Keller, J., LeBas, M. J., Sabine, P. A., *et al.* (1989) *A Classification of Igneous Rocks and Glossary of Terms.* Blackwell: Oxford.

Luis, J. F., Miranda, J. M., Galdeano, A., Patriat, P., Rossignol, J. C. & Mendes Victor, L. A. (1994) The Azores triple junction evolution since 10 Ma from aeromagnetic survey of the Mid-Atlantic Ridge. *Earth and Planetary Science Letters* **125**, 439–459.

Luis, J. F., Miranda, J. M., Galdeano, A. & Patriat, P. (1998) Constraints on the structure of the Azores spreading center from gravity data. *Marine Geophysical Researches* **20**.

Macdonald, G. A. (1968) Composition and origin of Hawaiian lavas. In: Coats, R. R., Hay, R. L. & Anderson, C. A. (eds) *Studies in Volcanology: A Memoir in Honor of Howel Williams.* Boulder, CO: Geological Society of America (GSA), pp. 477–522.

Montelli, R., Nolet, G., Dahlen, F. A., Masters, G., Engdahl, E. R. & Hung, S. H. (2004) Finite-frequency tomography reveals a variety of plumes in the mantle. *Science* **303**, 338–343.

Moore, R. B. (1990) Volcanic geology and eruption frequency, Sao Miguel, Azores. *Bulletin of Volcanology* **52**, 602–614.

Moore, R. B. (1991a) *Geologic Map of Sao Miguel, Azores.* Denver, CO: US Department of the Interior, US Geological Survey.

Moore, R. B. (1991b) Geology of three late Quaternary stratovolcanos on Sao Miguel, Azores. In: *US Geological Survey Bulletin.* US Geological Service.

Moore, R. B. & Rubin, M. (1991) Radiocarbon dates for Lava flows and pyroclastic deposits on Sao Miguel, Azores. *Radiocarbon* **33**, 151–164.

Nash, W. P. & Crecraft, H. R. (1985) Partition coefficients for trace elements in silicic magmas. *Geochimica et Cosmochimica Acta* **49**, 2309–2322.

Nelson, S. T. & Montana, A. (1992) Sieve-textured plagioclase in volcanic rocks produced by rapid decompression. *American Mineralogist* **77**, 1242–1249.

Nicholis, M. G. & Rutherford, M. J. (2004) Experimental constraints on magma ascent rate for the Crater Flat volcanic zone hawaiite. *Geology* **32**, 489–492.

Nielsen, R. L., Gallahan, W. E. & Newberger, F. (1992) Experimentally determined mineral–melt partition coefficients for Sc, Y and REE for olivine, orthopyroxene, pigeonite, magnetite and ilmenite. *Contributions to Mineralogy and Petrology* **110**, 488–499.

O'Nions, R. K., Hamilton, P. J. & Evensen, N. M. (1977) Variations in $^{143}Nd/^{144}Nd$ and $^{87}Sr/^{86}Sr$ ratios in oceanic basalts. *Earth and Planetary Science Letters* **34**, 13–22.

Pacheco, J. M., Quinterno, P. J., Gonçalves, P., Gasparon, M. & Ferreira, T. (2005) Sete Cidades Volcano (S. Miguel, Azores): constraints to eruptive scenarios. In: Union, E. G. (ed.) *EGU 2005.* Vienna: Geophysical Research Abstracts, p. 09772.

Pemberton, J. W. & Offler, R. (1985) Significance of clinopyroxene compositions from the Cudgegong Volcanics and Toolamanang Volcanics; Cudgegong–Mudgee District, NSW, Australia. *Mineralogical Magazine* **49**, 591–599.

Pichavant, M., Mysen, B. O. & Macdonald, R. (2002) Source and H (sub 2) O content of high-MgO magmas in island arc settings: an experimental study of a primitive calc–alkaline basalt from St. Vincent, Lesser Antilles arc. *Geochimica et Cosmochimica Acta* **66**, 2193–2209.

Putirka, K. (1997) Magma transport at Hawaii: inferences based on igneous thermobarometry. *Geology (Boulder)* **25**, 69–72.

Putirka, K. (1999) Clinopyroxene + liquid equilibria to 100 kbar and 2450 K. *Contributions to Mineralogy and Petrology* **135**, 151–163.

Putirka, K., Johnson, M., Kinzler, R., Longhi, J. & Walker, D. (1996) Thermobarometry of mafic igneous rocks based on clinopyroxene–liquid equilibria, 0–30 kbar. *Contributions to Mineralogy and Petrology* **123**, 92–108.

Putirka, K. D., Mikaelian, H., Ryerson, F. & Shaw, H. (2003) New clinopyroxene–liquid thermobarometers for mafic, evolved and volatile-bearing lava compositions, with applications to lavas from Tibet and the Snake River Plain, Idaho. *American Mineralogist* **88**, 1542–1554.

Reid, I. & Jackson, H. R. (1981) Oceanic spreading rate and crustal thickness. *Marine Geophysical Researches* **5**, 165–172.

Reiners, P. W. (1998) Reactive melt transport in the mantle and geochemical signatures of mantle-derived magmas. *Journal of Petrology* **39**, 1039–1061.

Reiners, P. W. (2002) Temporal–compositional trends in intraplate basalt eruptions: implications for mantle heterogeneity and melting processes. *Geochemistry, Geophysics, Geosystems* **3**, 1–30.

Renzulli, A. & Santi, P. (2000) Two-stage fractionation history of the alkali basalt–trachyte series of Sete Cidades volcano (Sao Miguel Island, Azores). *European Journal of Mineralogy* **12**, 469–494.

Ritsema, J. & Allen, R. M. (2003) The elusive mantle plume. *Earth and Planetary Science Letters* **207**, 1–12.

Roeder, P. L. & Emslie, R. F. (1970) Olivine–liquid equilibrium. *Contributions to Mineralogy and Petrology* **29**, 275–289.

Rutherford, M. J. & Devine, J. D. (1988) The May 18, 1980, eruption of Mount St. Helens; 3, Stability and chemistry of amphibole in the magma chamber. *Journal of Geophysical Research, B, Solid Earth and Planets* **93**, 11949–11959.

Rutherford, M. J. & Devine, J. D. (2003) Magmatic conditions and magma ascent as indicated by hornblende phase equilibria and reactions in the 1995–2002 Soufriere Hills magma. *Journal of Petrology* **44**, 1433–1454.

Rutherford, M. J. & Hill, P. M. (1993) Magma ascent rates from amphibole breakdown: an experimental study applied to the 1980–1986 Mount St. Helens eruptions. *Journal of Geophysical Research, B, Solid Earth and Planets* **98**, 19667–19685.

Sato, H. (1977) Nickel content of basaltic magmas: identification of primary magmas and a measure of the degree of olivine fractionation. *Lithos* **10**, 113–120.

Schilling, J.-G. (1975a) Azores mantle blob: rare-earth evidence. *Earth and Planetary Science Letters* **25**, 103–115.

Schilling, J.-G. (1975b) Rare-earth variations across 'normal segments' of the Reykjanes Ridge, 60°–53°N, Mid-Atlantic Ridge, 29°S, and East Pacific Rise, 2°–19°S, and evidence on the composition of the underlying low-velocity layer. *Journal of Geophysical Research* **80**, 1459–1473.

Schwarz, S., Kluegel, A. & Wohlgemuth, U. C. (2004) Melt extraction pathways and stagnation depths beneath the Madeira and Desertas rift zones (NE Atlantic) inferred from barometric studies. *Contributions to Mineralogy and Petrology* **147**, 228–240.

Searle, R. C. (1980) Tectonic pattern of the Azores spreading center and triple junction. *Earth and Planetary Science Letters* **51**.

Sleep, N. H. (1990) Hotspots and mantle plumes: some phenomenology. *Journal of Geophysical Research, B, Solid Earth and Planets* **95**, 6715–6736.

Sparks, S. R. J., Sigurdsson, H. & Wilson, L. (1977) Magma mixing: a mechanism for triggering acid explosive eruptions. *Nature* **267**, 315–318.

Stolper, E., Walker, D., Hager, B. H. & Hays, J. F. (1981) Melt segregation from partially molten source regions; the importance of melt density and source region size. *Journal of Geophysical Research* **B 86**, 6261–6271.

Storey, M., Wolff, J. A., Norry, M. J. & Marriner, G. F. (1989) Origin of hybrid lavas from Agua de Pau volcano, Sao Miguel, Azores. In: Saunders, A. D. & Norry, M. J. (eds) *Magmatism in the Ocean Basins. Geological Society Special Publication*, 161–180.

Thirlwall, M. F., Jenkins, C., Vroon, P. Z. & Mattey, D. P. (1997) Crustal interaction during construction of ocean islands: Pb–Sr–Nd–O isotope geochemistry of the shield basalts of Gran Canaria, Canary Islands. *Chemical Geology* **135**, 233–262.

Thompson, R. N. (1974) Some high-pressure pyroxenes. *Mineralogical Magazine* **39**, 768–787.

Turner, S., Hawkesworth, C., Rogers, N. & King, P. (1997) U–Th isotope disequilibria and ocean island basalt generation in the Azores. In: Hawkesworth, C. & Arndt, N. T. (eds) *Highlights of the Goldschmidt Meeting, in Honor of A. W. Hofmann*. Amsterdam: Elsevier, pp. 145–164.

Vogt, P. R. & Jung, W. Y. (2004) The Terceira Rift as hyper-slow, hotspot-dominated oblique spreading axis: a comparison with other slow-spreading plate boundaries. *Earth and Planetary Science Letters* **218**, 77–90.

Watson, S. & McKenzie, D. (1991) Melt generation by plumes: a study of Hawaiian volcanism. *Journal of Petrology* **32**, 501–537.

Whipkey, C. E., Capo, R. C., Chadwick, O. A. & Stewart, B. W. (2000) The importance of sea spray to the cation budget of a coastal Hawaiian soil: a strontium isotope approach. *Chemical Geology* **168**, 37–48.

White, W. M. & Hofmann, A. W. (1982) Sr and Nd isotope geochemistry of oceanic basalts and mantle evolution. *Nature* **296**, 821–825.

White, W. M., Schilling, J. G. & Hart, S. R. (1975) Sr-isotope geochemistry of the Azores and the Mid-Atlantic Ridge: 29 degrees N to 60 degrees N. *Eos, Transactions, American Geophysical Union* **56**, 471.

White, W. M., Tapia, M. D. M. & Schilling, J.-G. (1979) The petrology and geochemistry of the Azores Islands. *Contributions to Mineralogy and Petrology* **69**, 201–213.

Widom, E. (1991) Petrogenetic processes and timescales of young alkaline volcanic rocks, Sao Miguel, Azores. Doctoral thesis, University of California Santa Cruz.

Widom, E. & Shirey, S. B. (1996) Os isotope systematics in the Azores: implications for mantle plume sources. *Earth and Planetary Science Letters* **142**, 451–465.

Widom, E. & Farquhar, J. (2003) Oxygen isotope signatures in olivines from Sao Miguel (Azores) basalts: implications for crustal and mantle processes. *Chemical Geology* **193**, 237–255.

Widom, E., Schmincke, H. U. & Gill, J. B. (1992) Processes and timescales in the evolution of chemically zoned trachyte: Fogo A, Sao Miguel, Azores. *Contributions to Mineralogy and Petrology* **111**, 311–328.

Widom, E., Gill, J. B. & Schmincke, H. U. (1993) Syenite nodules as a long-term record of magmatic activity in Agua de Pau Volcano, Sao Miguel, Azores. *Journal of Petrology* **34**, 929–953.

Widom, E., Carlson, R. W., Gill, J. B. & Schmincke, H. U. (1997) Th–Sr–Nd–Pb isotope and trace element evidence for the origin of the Sao Miguel, Azores, enriched mantle source. *Chemical Geology* **140**, 49–68.

Wolff, J. A. (1984) Variation in Nb/Ta during differentiation of phonolitic magma, Tenerife, Canary Islands. *Geochimica et Cosmochimica Acta* **48**, 1345–1348.

Wolff, J. A., Grandy, J. S. & Larson, P. B. (2000) Interaction of mantle-derived magma with island crust? Trace element and oxygen isotope data from the Diego Hernandez Formation, Las Canadas, Tenerife. *Journal of Vocanology and Geothermal Research* **103**, 343–366.

Wones, D. R. & Gilbert, M. C. (1982) Chapter 3, Amphiboles in the igneous environment: introduction. In: Veblen, D. R. & Ribbe, P. H. (eds) *Amphiboles: Petrology and Experimental Phase Relations*. Washington, DC: Mineralogical Society of America, pp. 355–357.

Woodhead, J. D. (1992) Temporal geochemical evolution in oceanic intra-plate volcanics: a case study from the Marquesas (French Polynesia) and comparison with other hotspots. *Contributions to Mineralogy and Petrology* **111**, 458–467.

Zanetti, A., Tiepolo, M., Oberti, R. & Vannucci, R. (2004) Trace-element partitioning in olivine: modelling of a complete data set from a synthetic hydrous basanite melt. *Lithos* **75**, 39–54.